



1 **Impacts and uncertainties of climate-induced changes in** 2 **watershed inputs on estuarine hypoxia**

3
4 **Authors:** Kyle E. Hinson¹, Marjorie A.M. Friedrichs¹, Raymond G. Najjar²; Maria Herrmann²,
5 Zihao Bian³, Gopal Bhatt^{4,5}, Pierre St-Laurent¹, Hanqin Tian⁶, Gary Shenk^{7,5}

6
7 ¹Virginia Institute of Marine Science, William & Mary, Gloucester Point, VA 23062, USA

8 ²Department of Meteorology and Atmospheric Science, The Pennsylvania State University,
9 University Park, PA 16802, USA

10 ³International Center for Climate and Global Change, Auburn University, Auburn, AL 36849,
11 USA

12 ⁴Department of Civil & Environmental Engineering, The Pennsylvania State University, State
13 College, 16801, USA

14 ⁵United States Environmental Protection Agency Chesapeake Bay Program Office, Annapolis,
15 21401, USA

16 ⁶Schiller Institute for Integrated Science and Society, Department of Earth and Environmental
17 Sciences, Boston College, Chestnut Hill, MA 02467, USA

18 ⁷United States Geological Survey, Virginia/West Virginia Water Science Center, Richmond, VA
19 23228, USA

20

21 *Correspondence to:* Kyle E. Hinson (kehinson@vims.edu; kyle.e.hinson@gmail.com)

22 **Abstract**

23

24 Multiple climate-driven stressors, including warming and increased nutrient delivery, are
25 exacerbating hypoxia in coastal marine environments. Within coastal watersheds, environmental
26 managers are particularly interested in climate impacts on terrestrial processes, which may
27 undermine the efficacy of management actions designed to reduce eutrophication and consequent
28 low-oxygen conditions in receiving coastal waters. However, substantial uncertainty
29 accompanies the application of Earth System Model (ESM) projections to a regional modeling
30 framework when quantifying future changes to estuarine hypoxia due to climate change. In this
31 study, two downscaling methods are applied to multiple ESMs and used to force two
32 independent watershed models for Chesapeake Bay, a large coastal-plain estuary of the eastern
33 United States. The projected watershed changes are then used to force a coupled 3-D
34 hydrodynamic-biogeochemical estuarine model to project climate impacts on hypoxia, with
35 particular emphasis on projection uncertainties. Results indicate that all three factors (ESM,
36 downscaling method, and watershed model) are found to contribute significantly to the
37 uncertainty associated with future hypoxia, with the choice of ESM being the largest contributor.
38 Overall, in the absence of management actions, there is a high likelihood that climate change
39 impacts on the watershed will expand low-oxygen conditions by 2050, relative to a 1990s
40 baseline period; however, the projected increase in hypoxia is quite small (4%) because only
41 climate-induced changes in watershed inputs are considered and not those on the estuary itself.
42 Results also demonstrate that the attainment of established nutrient reduction targets will reduce
43 annual hypoxia by about 50% compared to the 1990s. Given these estimates, it is virtually



44 certain that fully implemented management actions reducing excess nutrient loadings will
45 outweigh hypoxia increases driven by climate-induced changes in terrestrial runoff.

46

47 **Short Summary**

48

49 Climate impacts are essential for environmental managers to consider when implementing
50 nutrient reduction plans designed to reduce hypoxia. This work highlights relative sources of
51 uncertainty in modeling regional climate impacts on the Chesapeake Bay watershed and
52 consequent declines in Bay oxygen levels. The results demonstrate that planned water quality
53 improvement goals are capable of reducing hypoxia levels by half, offsetting climate-driven
54 impacts to terrestrial runoff.



55 **1 Introduction**

56

57 Over the past several decades, estuarine and coastal ecosystems have been subject to elevated
58 levels of hypoxia relative to the open ocean (Gilbert et al., 2010), and are anticipated to be
59 affected by multiple climate change impacts including terrestrial runoff changes (Breitburg et al.,
60 2018) and rising temperatures (Whitney, 2022). Increases in precipitation volume and intensity
61 are likely to increase discharge and associated nutrient and sediment export to coastal systems
62 (Howarth et al., 2006; Lee et al., 2016; Sinha et al., 2017). Rising atmospheric temperatures will
63 increase soil temperatures and alter evapotranspiration, soil biogeochemical cycling and plant
64 responses (Schaefer and Alber, 2007; Wolkovich et al., 2012; Ator et al., 2022), also affecting
65 riverine nutrient export to marine habitats. Further changes to agricultural practices driven by
66 these same climate impacts are also likely to contribute to altered nutrient applications and
67 subsequent soil cycling (Wagena et al., 2018). Altogether, climate impacts in the terrestrial
68 environment may further eutrophy coastal ecosystems (Najjar et al., 2010), altering the
69 phenology and biogeochemical rates of nutrient consumption and exacerbating hypoxia (Testa et
70 al., 2018).

71 Future estimates of coastal hypoxia have increased substantially over the past decade, likely
72 influenced by increased access to biogeochemical modeling tools and regional climate
73 projections needed for finer scale modeling and analyses (Fennel et al., 2019). The majority of
74 coastal hypoxia climate impact studies have focused on a select few coastal locations including
75 the Baltic Sea (Meier et al., 2011a,b; Meier et al., 2012; Neumann et al., 2012; Ryabchenko et
76 al., 2016; Saraiva et al., 2019a,b; Wählström et al., 2020; Meier et al., 2021; Meier et al., 2022),
77 Chesapeake Bay (Wang et al., 2017; Irby et al., 2018; Ni et al., 2019; Testa et al., 2021; Tian et
78 al., 2021; Cai et al., 2021), and the Gulf of Mexico (Justić et al., 1996; Justić et al., 2007; Lehrter
79 et al., 2017; Laurent et al., 2018). Other projected changes to dissolved oxygen (O₂) levels have
80 been documented in nearshore environments including the North Sea (Meire et al., 2013;
81 Wakelin et al., 2020), Arabian Sea (Lachkar et al., 2019), California Current System (Dussin et
82 al., 2019; Siedlecki et al., 2021; Pozo Buil et al., 2021), and coastal waters surrounding China
83 (Hong et al., 2020; Yau et al., 2020; Zhang et al., 2021; Zhang et al., 2022). Hypoxia projections
84 in relatively smaller estuaries have also been documented in the Elbe (Hein et al., 2018),
85 Garonne (Lajaunie-Salla et al., 2018), and Long Island Sound (Whitney and Vlahos, 2021).

86 Broadly speaking, these climate impact studies apply either a range of idealized changes to
87 conduct a sensitivity study or utilize long-term projections derived from Earth System Models
88 (ESMs) (IPCC, 2013). When directly applying such projections to study regional coastal oxygen
89 responses, dynamically or statistically downscaled estimates of atmospheric and marine variables
90 are typically used to continuously simulate climate impacts or to calculate and apply a change
91 factor (Carter et al., 1994; Anandhi et al., 2011) to a shorter historical time period. Quantifying
92 the relative uncertainties from various sources including ESM, downscaling methodology,
93 internal variability, and hydrological model is not new to the field of climate research (Hawkins
94 and Sutton, 2009; Yip et al., 2011; Northrop and Chandler, 2014) or watershed applications
95 (Bosshard et al., 2013; Vetter et al., 2017; Wang et al., 2020; Ohn et al., 2021). Questions of
96 uncertainty due to climate effects in past marine ecosystem impact studies have often been
97 addressed by selecting some combination of ESMs and/or emissions scenarios (Meier et al.,
98 2011a; Ni et al., 2019; Saraiva et al., 2019b; Meier et al., 2019; Meier et al., 2021; Pozo Buil et
99 al., 2021). Additionally, some studies have also sought to account for the importance of managed
100 nutrient runoff from terrestrial (Irby et al., 2018; Saraiva et al., 2019a) and atmospheric (Yau et



101 al., 2020; Meier et al., 2021) sources and their impacts on oxygen levels. Despite some
102 comprehensive efforts to identify sources of uncertainty in coastal oxygen projections (Meier et
103 al., 2019; 2021), few studies have evaluated uncertainties introduced by the choice of specific
104 downscaling method and/or terrestrial model. These factors represent additional sources of
105 variability when estimating future hypoxia and are inherent in regional simulations of coastal
106 dynamics.

107 The Chesapeake Bay, which is the largest estuary in the continental United States (Kemp et
108 al., 2005), has undergone intensive management efforts to improve water quality and oxygen
109 levels over the past three decades. These management efforts have focused on the reduction of
110 excess nitrogen, phosphorus, and sediment loadings to the Bay (USEPA, 2010), and continuous
111 adaptive monitoring efforts to evaluate progress in restoring water quality (Tango and Batiuk,
112 2016). Recent analyses of monitoring data have demonstrated improvements in water quality
113 throughout the Bay despite the trajectory of recovery being slowed by extreme weather events
114 (Zhang et al., 2018). Observed lags in water quality responses to nutrient reductions (Murphy et
115 al., 2022) are also evident in recent years (Zahran et al. 2022). Despite the difficulties in
116 assessing long-term improvements in water quality due to strong interannual variability, new
117 research has demonstrated that the Chesapeake Bay is more resilient to recent and ongoing
118 climate change impacts that have decreased oxygen levels as a result of decades of nutrient load
119 reductions (Frankel et al., 2022).

120 In recent years managers have recognized the importance of investigating whether the
121 originally established Total Maximum Daily Loads (USEPA, 2010) will need to be adjusted to
122 ensure the attainment of water quality standards for the Chesapeake Bay as the climate changes
123 (Chesapeake Bay Program, 2020; Hood et al., 2021). Increasing temperatures and precipitation
124 are anticipated to affect watershed snowpack, soil moisture levels, terrestrial nutrient cycling,
125 and associated discharge, streamflow generation, and flooding (Shenk et al., 2021b), potentially
126 altering the efficacy of nutrient reduction strategies. Increases in nutrient and carbon inputs to the
127 Bay resulting from climate change and anthropogenic stressors have already been documented
128 over the course of the past century (Pan et al., 2021; Yao et al., 2021), and are anticipated to
129 increase in the 21st century as well (Wang et al., 2017; Irby et al., 2018; Ni et al., 2019). For
130 example, Irby et al. (2018) directly tested the role of future nutrient reductions via a sensitivity
131 analysis of mid-century climate effects, and found substantial alleviation of hypoxic conditions
132 when management targets were met, despite significantly increasing water temperatures.
133 However, that study applied spatially constant changes in watershed inputs derived from a
134 specific watershed model, one downscaling technique and a median estimate of ESM
135 projections. A more robust effort to produce a range of scenarios incorporating multiple
136 watershed models, downscaling techniques and ESMs is needed to assess uncertainty estimates
137 of projected hypoxia, which can be used to guide decision-making that explicitly considers what
138 levels of environmental risk are acceptable for Chesapeake Bay stakeholders.

139 The present study applies multiple downscaled ESMs to two independently developed
140 watershed models with significantly different representation of watershed processes and spatial
141 scale; both are used to force a coupled hydrodynamic-biogeochemical estuarine model in order
142 to better constrain the relative uncertainties of future terrestrial runoff estimates on estuarine
143 hypoxia (Shenk et al., 2021a). The resulting ensemble of numerical experiments includes
144 realistic climate forcings and an extensive set of regional linked watershed-estuarine
145 deterministic model simulations. The framework established in this research assesses the relative
146 uncertainties introduced by choice of ESM, downscaling methodology, and regionally focused



147 watershed model in quantifying changes to O₂ levels in the estuary. Additionally, this
148 investigation constrains the bounds of changes to Chesapeake Bay hypoxia (defined herein as O₂
149 < 2 mg L⁻¹) with and without the effects of management actions, using an ensemble of realistic
150 watershed forcings. The study provides a roadmap for environmental managers to design climate
151 impact assessments that are better able to quantify the range of possible future levels of hypoxia,
152 which can be influenced by nutrient management actions.

153

154 **2 Methods**

155

156 **2.1 Monitoring data**

157 Monthly estimates of freshwater discharge, inorganic nitrogen, and organic nitrogen at the
158 non-tidal monitoring stations nearest the head of tide of the three largest tributaries to the
159 Chesapeake Bay (Susquehanna, Potomac, and James; Fig. 1a; Table S1) were used to evaluate
160 the performance of watershed models. Discharge and nitrogen load estimates are derived from
161 observations that are collected at United States Geological Survey (USGS) stream gages and
162 comprise part of the USGS River Input Monitoring (RIM) program in the Chesapeake Bay
163 watershed. Estimates for the nitrogen species were calculated using a weighted statistical
164 regression process that accounts for the variability introduced by time, discharge, and season
165 (Hirsch et al., 2010).

166 Main stem bay observations collected over the period 1991-2000, accessible via a data
167 repository maintained by the Chesapeake Bay Program (CBP; Olson 2012; CBP DataHub 2020),
168 were used to assess estuarine model skill (see Sect. 2.3.1). Since 1984, numerous water quality
169 data have been collected along the Bay's main stem and throughout its tributaries at semi-
170 monthly to monthly intervals as part of the Water Quality Monitoring Program (WQMP). These
171 data were collected at the surface, above and below the pycnocline, and at the bottom for
172 chemical variables including nitrate and organic nitrogen, and throughout the entire water
173 column at 1-2 m intervals for O₂. Twenty CBP stations were selected for model comparison at
174 the surface and bottom (Fig. 1b, Table S2), including those most frequently sampled and those
175 located along the entirety of the Bay's main channel where hypoxia commonly occurs (Officer et
176 al., 1984; Hagy et al., 2004). Estimates of annual hypoxic volume (AHV), defined as the volume
177 of hypoxic water integrated over the year (with units of volume*time), were taken from the
178 Bever et al. (2013; 2018; 2021) interpolation of O₂ measurements at 56 CBP stations.

179

180 **2.2 Estuarine and watershed modeling tools and evaluation**

181 Model simulations are conducted with ChesROMS-ECB, a fully coupled, three-dimensional,
182 hydrodynamic and Estuarine Carbon Biogeochemistry (ECB) implementation of the Regional
183 Ocean Modeling System (ROMS) developed for the Chesapeake Bay with 20 terrain-following
184 vertical levels and an average horizontal resolution of approximately 1.8 kilometers in the
185 estuary's mainstem (Feng et al., 2015; St-Laurent et al., 2020; Frankel et al., 2022). Two
186 parameter changes were recently made to improve the representation of modeled oxygen: (1) a
187 decrease of the maximum growth rate of phytoplankton, which, following Irby et al. (2018),
188 preserves the temperature-dependent linear Q₁₀ described in Lomas et al. (2002), and (2) a
189 decrease in the critical bottom shear stress from 0.010 Pa to 0.007 Pa, which increases the
190 resuspension of organic matter and is well within the range of observed shear stresses evaluated
191 by Peterson (1999).



192 Estimates of watershed discharge, nitrogen loading, and sediment loading to drive the
193 estuarine model were obtained via two independently developed models of the Chesapeake Bay
194 watershed: the Dynamic Land Ecosystem Model (DLEM; Yang et al., 2015; Yao et al., 2021)
195 and the USEPA Chesapeake Bay Program’s regulatory Phase 6 Watershed Model (Phase 6;
196 Chesapeake Bay Program, 2020). Both models were applied to generate comparable reference
197 runs over the average hydrology period of 1991-2000, chosen because it reflects the decade used
198 by the Chesapeake Bay Program to calculate Total Maximum Daily Loads (USEPA, 2010) and
199 assess water quality improvements. Outputs from both watershed models were aggregated into
200 10 major river input locations (Fig. 1). Watershed outputs were mapped to estuarine variables as
201 in Frankel et al. (2022), except that a more realistic partitioning of terrestrial organic nitrogen
202 loading into labile and refractory pools was implemented such that the percent refractory organic
203 nitrogen loading increases with discharge at high flow volumes (Appendix A).

204 Atmospheric conditions, including temperature and winds, were obtained from the ERA5
205 reanalysis dataset (C3S, 2017) as in Hinson et al. (2021). Coastal boundary conditions were
206 interpolated to match the nearest physical and nutrient observations, as in previous work (Da et
207 al., 2021). In order to isolate the impacts of climate-driven changes in watershed inputs,
208 atmospheric and coastal boundary conditions were kept the same in all model simulations under
209 realistic 1991-2000 conditions, for both reference runs (1991-2000) and all future scenarios
210 (2046-2055).

211 Watershed and estuarine model skill was evaluated by comparing results from the two
212 reference scenarios to available data (see Sect. 2.1). Nash–Sutcliffe efficiencies (Nash and
213 Sutcliffe, 1970) were used to evaluate watershed model performance of freshwater discharge and
214 nutrient loadings. Estuarine model skill was evaluated by comparing model outputs matching the
215 spatio-temporal variability of observations at 20 main stem stations over the 10-year reference
216 period. Average bias (model output minus observed value) and root-mean squared difference
217 (RMSD) of annual O₂, nitrate (NO₃), and dissolved organic nitrogen (DON) concentrations were
218 calculated at the surface and bottom. AHV estimates were calculated by summing the daily
219 volume of model cells containing low-oxygen waters (O₂ < 2 mg L⁻¹), and are expressed in units
220 of km³ d following Bever et al. (2013; 2018; 2021). Daily net primary production estimates were
221 integrated over the entire water column and averaged across the Bay and month before being
222 compared to average Bay-wide estimates from Harding et al. (2002).

223

224 **2.3 Projected changes in atmospheric temperature and precipitation**

225 Mid-21st century projected changes in atmospheric temperature and precipitation under a
226 high emissions scenario (RCP 8.5) were obtained for multiple CMIP5 ESMs that were regionally
227 downscaled via two statistical methodologies: Multivariate Adaptive Corrected Analogs
228 (MACA; Abatzoglou and Brown, 2012; downloaded from MACAv2-METDATA) and Bias-
229 Corrected Spatial Disaggregation (BCSD; Wood et al., 2004; downloaded from Reclamation,
230 2013). (Note that downscaled CMIP5 ESM output was used because downscaled CMIP6 ESM
231 output was not yet available when the research began.) Downscaled MACA and BCSD
232 projections have an average spatial resolution of approximately 0.042° and 0.125°, respectively.
233 A delta approach (Prudhomme et al., 2002; Anandhi et al., 2011) was used to estimate the
234 absolute change in atmospheric temperature and fractional change in precipitation over the
235 Chesapeake Bay watershed. In this delta approach (also commonly referred to as a perturbation
236 method or change-factor method), the difference in a given climate variable (i.e., air temperature
237 or precipitation) is calculated by first subtracting monthly downscaled ESM estimates averaged



238 over a hindcast period (in this case 1981-2010) from average monthly future projections (in this
239 case 2036-2065). The resulting mean annual cycle (with monthly resolution) in the delta (i.e., the
240 absolute change in temperature or fractional change in precipitation) is then applied to reference
241 atmospheric forcing inputs (in this case for 1991-2000) to generate future watershed scenarios
242 (in this case for 2046-2055, hereafter referred to as mid-century) and limit uncertainty introduced
243 by interannual variability. An additional step to modify precipitation intensity is also included in
244 all climate scenarios, following the methodology outlined in Shenk et al. (2021b). Thirty-year
245 averaging periods were used to limit potential biases introduced by multidecadal oscillations.

246 To reduce the computational load of applying the dozens of available ESMs to our combined
247 watershed-estuarine modeling framework for a full factorial experiment, the Katsavounidis-Kuo-
248 Zhang (KKZ; Katsavounidis et al., 1994) algorithm was applied to select a subset of five ESMs
249 from both downscaled datasets. KKZ is an objective procedure for selecting a subset of members
250 that best span the spread of the full ensemble in a multivariate space. The selection process
251 incrementally adds members to the ones previously selected, so that the entire ensemble is
252 ordered and a subset of any size can be selected. This method has proven effective at covering
253 the largest range of outcomes using the fewest ESMs in watersheds across the United States in
254 previous research (Ross and Najjar, 2019). Because changes to hypoxia must be computed after a
255 subset of ESMs are selected, the downscaled results were classified in terms of changes to the
256 two variables most likely to influence hypoxia: air temperature from May–October (i.e., the
257 historic hypoxic season in Chesapeake Bay) and precipitation from November–June
258 (corresponding to the highest set of correlation coefficients when regressed against historical
259 AHV estimates; Supplementary Material; Fig. S1). The KKZ algorithm first selected an ESM
260 nearest to the center of the cluster of models in the two-parameter space, which is referred to
261 hereafter as the Center ESM, before iteratively selecting additional ESMs that were furthest from
262 the center of the distribution and other previously selected ESMs (Fig. 2, Table S3). The next
263 four selected ESMs are referred to as Hot/Wet, Cool/Wet, Hot/Dry, and Cool/Dry ESMs to
264 denote whether they are cooler, hotter, wetter, or drier, relative to the Center ESM. The specific
265 ESMs selected based on MACA and BCSD differ slightly; however, three of the five models are
266 the same (Cool/Dry, Hot/Dry, and Cool/Wet). This ESM selection process allows for a more
267 robust comparison of the distribution of ESMs from multiple downscaled datasets as opposed to
268 individual ESM comparisons that may privilege one downscaling method over others. However,
269 because inexact matches among ESMs can impact the quantification of relative uncertainty
270 (Sect. 2.5), additional scenarios were simulated as needed for the Center and Hot/Wet ESMs,
271 which were different for the two downscaling techniques (Fig. 2, Table S3). Future change in
272 temperature and precipitation between the two downscaling methods are shown for the Center
273 ESM (Fig. 3); changes for the other four ESMs are found in the Supplementary Material (Fig.
274 S2).

275

276 2.4 Experiments

277 Three numerical experiments (sets of simulations) were conducted to evaluate the impacts of
278 climate scenario factors, management conditions, and the use of a subset of ESMs on future
279 AHV projections and uncertainty (Table 1). To isolate climate impacts on AHV from the
280 watershed alone, direct atmospheric and oceanic forcings to the Bay were held the same as in the
281 reference simulations (see Sect. 2.3) for all experiments. The first experiment (Multi-Factor)
282 evaluates the relative change in AHV (hereafter defined as Δ AHV) between the 1991-2000 and
283 2046-2055 time periods due to the following factors: ESM, downscaling method, and watershed



284 model (Table 1, Fig. 4). Atmospheric deltas from ten downscaled ESMs (five from MACA and
285 five from BCSD) were applied directly to the two watershed models for a total of 20 simulations.
286 A separate Phase 6 climate-reference run is used to evaluate the impacts of climate alone by
287 holding land use and nutrient applications constant. This differs slightly from the Phase 6
288 reference run that simulates realistic and interannually varying nutrient inputs and terrestrial
289 conditions and is compared against observations (Sect. 2.2). Two additional simulations were
290 conducted with Phase 6 to account for the fact that the ESMs selected by the KKZ method were
291 not identical for MACA and BCSD (Table 1, Fig. 2).

292 The second experiment (Management) applied the same deltas used for Phase 6 MACA
293 scenarios in the Multi-Factor experiment, but also included the effect of changing environmental
294 management conditions, for a total of five additional simulations. These Management
295 simulations assume that reduction targets for nutrient and sediment runoff are met in accordance
296 with established management goals (USEPA, 2010). One additional scenario was conducted in
297 which management goals were imposed, and climate change was not.

298 The third experiment (All ESMs) applied all 20 MACA downscaled ESM deltas to the
299 DLEM scenarios without any changes to management conditions, for a total of 20 additional
300 simulations. Comparing the results of the first (Multi-Factor) and third (All ESMs) experiments
301 highlights the strengths and limitations of using a subset of ESMs.

302

303 **2.5 Climate scenario analyses**

304 To analyze climate impacts on Chesapeake Bay hypoxia, changes in O₂ and AHV were
305 compared between the reference runs and the future simulations. Relative O₂ impacts introduced
306 by the three climate scenario factors (ESM, downscaling method, and watershed model) were
307 determined by applying an analysis of variance (ANOVA) approach to average Δ AHV estimates
308 for each climate scenario. This method has been previously applied to the quantification of
309 uncertainty sources in climate and hydrological applications (Hawkins and Sutton, 2009; Yip et
310 al., 2011; Bosshard et al., 2013; Ohn et al., 2021). To use this method in this study, an average
311 annual metric is first calculated for an outcome of interest (i.e., change in discharge, nitrogen
312 loading, or hypoxic volume) within the Multi-Factor experiment. Then, the relative uncertainty is
313 determined by calculating the sum of squares due to individual effects for each experimental
314 factor (ESM, downscaling method, or watershed model). Following Ohn et al. (2021), the
315 cumulative uncertainty is quantified for successive uncertainties introduced by each factor as
316 well as their interactions, removing the unexplained interaction term described in Bosshard et al.
317 (2013). The two additional ESM scenarios described previously (Table 1, Table S3) were used
318 due to the inexact matches between MACA and BCSD ESMs selected by KKZ. Despite five
319 ESMs being used in combination with only two downscaling methods and two watershed models
320 in this analysis, the approach outlined (Bosshard et al., 2013; Ohn et al., 2021) accounts for this
321 factor imbalance (five vs. two) by repeatedly subsampling combinations of two ESM scenarios
322 from the five available.

323 Relative frequency histograms and cumulative distributions were used to quantify the overall
324 likelihoods of increasing/decreasing Δ AHV across the entire range of future scenarios. Average
325 changes in the spatial distribution of O₂ over the typical hypoxia season (May–September) were
326 compared among all climate scenarios with no changes to management conditions. Results were
327 considered significant if at least 80% of model scenarios tested agree on the direction of O₂
328 change in the estuary, as in Tebaldi et al. (2011).

329



330 **3 Results**

331

332 **3.1 Model Skill**

333

334 **3.1.1 Watershed Models**

335

336 Modeled discharge, nitrate loading, and organic nitrogen loading from the three largest Bay
337 tributaries are comparable to observed monthly estimates derived from weighted statistical
338 regressions (see Sect. 2.1). At the most downstream USGS stations on the Susquehanna,
339 Potomac, and James Rivers, both Phase 6 and DLEM discharge estimates have higher skill
340 (Nash–Sutcliffe Efficiencies closer to 1.0) relative to nitrate and organic nitrogen loading
341 estimates (Table 2, Fig. S3). Although the overall skill of Phase 6 and DLEM is similar, Phase 6
342 generally exhibits higher model skill than DLEM in estimating monthly nitrate loading, while
343 DLEM demonstrates greater skill in simulating organic nitrogen loading.

344

345 **3.1.2 Estuarine Model**

346

347 The two reference simulations, forced with loadings from DLEM and Phase 6, demonstrate
348 substantial skill in representing key main stem estuarine biogeochemical variables, including O₂,
349 NO₃, DON, primary production, and AHV (Table 3) throughout the Bay’s mainstem. Overall, all
350 modeled variables at the surface and bottom forced by both DLEM and Phase 6 lie within 1
351 standard deviation of observations. Modeled O₂ is slightly greater than spatio–temporally paired
352 observations at the bottom, and slightly lower than observations at the surface throughout the
353 entire year (Table 3) and in the summer period of hypoxia (Fig. 5a-b), leading to a bias that is
354 relatively small compared to the standard deviations of observed O₂ concentrations across the
355 entire year (Table 3). Additionally, modeled O₂ performs similarly to or better than the results
356 included in the multi-model comparison presented in Irby et al. (2016). Modeled average annual
357 NO₃ and DON are also within the range of observations at both the surface and bottom (Table 3).
358 Whole Bay net primary production agrees well with observed estimates (Harding et al., 2002)
359 reported over a similar time period (Table 3). Finally, modeled AHV compares favorably to data-
360 derived interpolated estimates (Table 3; Fig. 5c), with increased hypoxia in wet years compared
361 to dry years. Average AHV estimates using Phase 6 and DLEM inputs are, respectively, 16%
362 and 26% greater than interpolated observations (Table 3; Fig. 5c) and approximately half the
363 model estimates lie within the estimated uncertainties (RMS % error) of the interpolation
364 methodology ($\pm 13\%$; Bever et al., 2018). Model estimates of AHV are generally slightly greater
365 when ChesROMS-ECB is forced by DLEM watershed outputs as opposed to those from Phase 6
366 (Table 3; Fig. 5c).

367

368 **3.2 Future (mid-21st century) projections of watershed discharge and nutrient loading**

369

370 Increasing temperatures and changing precipitation throughout the Bay watershed produce
371 different discharge responses for the two watershed models. On average, Phase 6 climate
372 scenarios increase watershed runoff relative to the reference run by 4-6% while DLEM climate
373 scenarios decrease average flow by 1-4% (Table 4). The annual flow changes range from -12 to
374 +15% among ESM scenarios, with wetter ESMs tending to increase annual watershed discharge
375 while drier ESM scenarios generally decrease average watershed runoff, with a lesser impact due



376 to atmospheric warming (Table 4; Fig. 6a). For both watershed models and downscaling
377 methods, the Cool/Wet ESM produces the greatest increase in annual discharge. Overall, the
378 greatest variability in changes to discharge estimates is due to ESM, as MACA and BCSD
379 scenarios increase or decrease annual discharge by comparable amounts (Table 4; Fig 6a).

380 Chesapeake Bay Phase 6 watershed model climate scenarios increase average annual total
381 nitrogen (TN) by +30% and +45% for MACA and BCSD respectively, but do not substantially
382 change DLEM TN loads (+1% and -2% for MACA and BCSD, respectively; Fig. 7). Greater
383 Phase 6 TN loadings are primarily due to extreme values in the Cool/Wet climate scenarios and
384 are driven by increases in refractory DON (Fig. 7a). While DLEM scenarios show increases in
385 the percentage of inorganic nitrogen and labile organic forms of total nitrogen loads, the
386 contribution of particulate organic nitrogen (PON) decreases, resulting in little to no increases in
387 overall TN loading (Fig. 7a). Phase 6 produces wetter climate scenarios increasing TN loading
388 more than drier scenarios (Table 4; Fig 6b), with this effect being most pronounced for the
389 Cool/Wet ESM. Phase 6 also produces the greatest percent changes in the southern rivers (James,
390 York, Rappahannock), while DLEM produces similar percent changes in all rivers (Fig. 7b).
391 Some Phase 6 climate scenarios substantially increase the average loading change in smaller
392 watersheds like the Rappahannock and York, which increase TN between 77-172% and 32-
393 430%, respectively, and are comparable to the absolute change in Susquehanna TN loading (Fig.
394 7b). In contrast with the Multi-Factor experiment results, climate scenarios that include
395 management actions substantially reduce TN loading (-28%; Fig. 7, Table 4). Like other Phase 6
396 climate scenarios that don't account for management actions, the proportion of refractory organic
397 nitrogen increases for the climate scenarios with management (+49%), but in these cases the
398 average labile inorganic and organic nitrogen loadings also substantially decrease (-40%).
399

400 **3.3 Effects of future watershed change on estuarine O₂**

401
402 Climate change impacts on watershed discharge and nitrogen loading substantially affect
403 estuarine hypoxia, even when, as in this study, direct climate effects on the Bay are not
404 considered. On average, the Multi-Factor climate scenarios decrease average summer bottom O₂
405 in the Bay's mainstem while also slightly increasing O₂ at the surface in some mid-Bay areas
406 (Fig. 8). In the northern part of the mainstem near the Susquehanna River outfall, model results
407 show consistent decreases in both bottom and surface summer O₂ (Fig. 8e,f). Further down the
408 main stem in the mid-Bay, surface O₂ increases in wet years, and experiences almost no change
409 in dry years (Fig. 8b,c). In the same region, bottom O₂ declines less during wet years and
410 worsen during dry years (Fig. 8e,f). Increasing O₂ levels are found in the shallow portions of the
411 major tidal tributaries (i.e., Potomac and James), but are more pronounced in wet years than dry
412 years (Fig. 8b-c,e-f). Altogether, average summer surface O₂ increases by $0.02 \pm 0.03 \text{ mg L}^{-1}$
413 (average change and standard deviation) while bottom O₂ decreases by $0.03 \pm 0.06 \text{ mg L}^{-1}$.

414 There are some clear distinctions in the overall changes to future AHV when evaluating all
415 Multi-Factor experiments. Climate effects on the watershed in DLEM increase AHV more so
416 than in Phase 6 (5.6% vs 3.1%, respectively), but the overall standard deviation of DLEM Δ AHV
417 results are greater than those for Phase 6 (Table 5). Similarly, using MACA vs. BCSD results in
418 greater changes in Δ AHV (4.8% vs. 3.9%), albeit this difference due to the choice of
419 downscaling method is less than that due to the choice of watershed model. Depending on the
420 choice of ESM, Δ AHV ranges between +0.9% (for the Cool/Dry ESM) to +8.3 % (for the
421 Cool/Wet ESM) with the Center ESM producing intermediate results (+4.4 %). When comparing



422 the impact of a particular ESM, wetter models tend to produce greater Δ AHV than drier
423 scenarios (Fig. 6c), although interannual variability is still large. When climate scenarios are
424 downscaled using different methodologies (either MACA or BCSD), average Δ AHVs have some
425 notable differences, e.g., applying the Cool/Dry model to Phase 6 produces opposite average
426 changes to hypoxia depending on downscaling method (Fig. 6c). Considering all possible
427 combinations of scenarios, ESM average annual projected AHV spans a range of 921-939 km³ d
428 for Phase 6 and 1019-1049 km³ d for DLEM, and four out of five of the climate scenarios in the
429 Multi-Factor experiment projecting increases in average AHV (Table 4).

430 When the full distribution of Multi-Factor scenarios is evaluated, the average and standard
431 deviation of these annual Δ AHV results are estimated to be 37 ± 64 km³ d ($4.4 \pm 7.4\%$; Fig 9).
432 Wetter ESMs (blues in Fig. 9a) are more likely to increase hypoxia compared to drier ESMs,
433 despite differences in downscaling method or watershed model. The likelihoods of the Cool/Dry
434 or Hot/Dry ESM increasing hypoxia are only 58% or 50%, respectively, but these chances are
435 greater than 80% for the Center, Hot/Wet, and Cool/Wet ESMs (Fig. 9a). Altogether, the Multi-
436 Factor experiment results in 72% of the runs increasing AHV when considering climate change
437 impacts on terrestrial runoff (Fig. 9b). (Note, however, that this cannot technically be considered
438 to be a statistical probability as the KKZ selection process used to generate our sample of climate
439 scenarios is neither random nor independent.)

440 The All-ESMs experiment produces similar results to those obtained when only a subset of
441 five ESMs are used. Specifically, Δ AHV increases by $6.3 \pm 3.5\%$ using only five KKZ-selected
442 ESMs and by $9.6 \pm 1.7\%$ when using all 20 ESMs (Fig. 10a,b; Model IDs further defined in
443 Table S3). The use of five KKZ-selected ESMs covers approximately 69% of the total range of
444 all 20 ESMs (Fig. 10c). Despite more than 15,000 options to choose from when selecting five out
445 of 20 ESMs, the subset selected in this work demonstrates an improved ability to outperform a
446 random selection of five ESMs (Fig. 10c) and generates a useful range of hypoxia projections.

447 The results of the Management experiment demonstrate the substantial impact of future
448 nutrient reductions on hypoxia, decreasing average AHV by $50 \pm 7\%$ relative to the 1990s
449 (Δ AHV = -438 ± 47 km³ d; Table 4; Fig. 11). Because there is a linear relationship between
450 Δ AHV computed with Phase 6 MACA scenarios including management actions (Δ AHV_{mgmt}) and
451 those without (Δ AHV = $0.56 * \Delta$ AHV<sub>mgmt} - 262; $R^2=0.59$, Fig. S5), Δ AHV_{mgmt} can be estimated
452 for any scenario by applying this linear model to the non-management scenario distribution. The
453 result is a decrease of approximately 417 ± 67 km³ d among all scenarios, within the range of the
454 management scenario subset obtained here by applying only MACA downscaled ESMs to Phase
455 6. As expected, hypoxia increases in the Management experiment when climate impacts are also
456 included relative to the reference management scenario, specifically by 17.1 ± 34.8 km³ d or 3.8
457 $\pm 7.8\%$ (Table 4; Fig 6c).</sub>

458

459 3.4 Contributions to Climate Scenario Uncertainty

460

461 Applying an ANOVA approach (Ohn et al., 2021) to watershed discharge, nutrient loadings,
462 and Δ AHV within the Multi-Factor experiment reveals that the relative uncertainties introduced
463 by the choice of ESM, downscaling method, and watershed model vary substantially (Fig. 12).
464 The choice of ESM is the dominant factor affecting changes to watershed discharge and nutrient
465 loadings (Fig. 12a-c), and comprises 59-74% of the total uncertainty. The choice of watershed
466 model is the next largest source of uncertainty, making up 17-34% of the total variance in
467 watershed changes, while the downscaling method only contributes 3-14%. Uncertainty in



468 projected organic nitrogen loadings is particularly affected by the choice of watershed model,
469 overwhelming the variability introduced by downscaling method, and strongly affecting
470 estimates of total nitrogen change. Unlike changes to watershed flow and loadings, the
471 uncertainty of projected changes to hypoxia is much more evenly distributed among the three
472 scenario factors: 40%, 25%, and 35%, for ESM, downscaling method, and watershed model
473 respectively (Fig. 12d).

474

475 **4 Discussion**

476

477 **4.1 Watershed Climate Scenario Impacts on Riverine Export and Hypoxia**

478

479 The climate scenario projections evaluated in this study are in near complete agreement that
480 the Chesapeake Bay watershed will be warmer and experience greater levels of precipitation by
481 mid-century, yet these results are not as straightforward to interpret as they relate to changes in
482 discharge, nutrient loads, and estuarine hypoxia. Climate impacts on extreme river flows are
483 currently evident at global scales (Gudmundsson et al., 2021), and projected increases in
484 precipitation that could shape such events are aligned with estimates for this region derived from
485 observational (Yang et al., 2021) and modeling (Huang et al., 2021) studies, as well as for other
486 regions at similar latitudes (Bevacqua et al., 2021; Madakumbura et al., 2021). However,
487 differences exist in the spatial distribution and timing of these precipitation increases, as well as
488 in the temperature-affected rates of evapotranspiration. As a result, these estimates produce
489 varied projections for future freshwater discharge. These complex interactions make it difficult
490 to directly predict future discharge from projected precipitation changes, and even more difficult
491 to relate these to changes in nutrient loading. For example, in this study half of the climate
492 scenarios produce increasing discharge on an annual basis, yet more than 75% of these scenarios
493 increase total nitrogen loading. Differences in the representation of soil and riverine nitrogen
494 processes between watershed models also results in inconsistent simulated responses of nitrogen
495 export to similar precipitation rates. Disparate export of nitrogen species (i.e., nitrate and organic
496 nitrogen) between watershed models also directly affects future nutrient load projections. These
497 hydrological model differences are evidenced by DLEM's higher NO₃ outputs that offset lower
498 organic nitrogen loadings (Fig. 7a), and are discussed further in depth in Sect. 4.2.

499 Our analysis quantifies changes in hypoxia due to mid-century climate change impacts on
500 watershed hydrologic and water quality responses, and provides an estimate of the relative
501 uncertainty in estuarine hypoxia response due to three distinct factors (Fig. 12): Earth System
502 Model, downscaling method, and watershed model. Our experimental findings suggest that, in
503 the absence of management actions, mid-century climate impacts on the Chesapeake Bay
504 watershed will increase hypoxia, specifically annual hypoxic volume (AHV), by an average of 4
505 \pm 7%, but changes to Bay O₂ levels vary spatially. Average bottom main stem O₂ levels from
506 May–September are expected to decrease most in the southern half of the Bay (south of 38.5°N),
507 particularly in climatologically dry years (Fig. 8). Again, it is important to remember that these
508 spatially varying changes only account for the effects of climate change on watershed response
509 in isolation, and do not include the additional direct impacts of the atmosphere and ocean. While
510 previous findings by Irby et al. (2018) suggest that increasing atmospheric temperatures are
511 likely to uniformly decrease O₂ levels throughout the Bay's main stem, increasing temperatures
512 at the ocean boundary during warmer months when hypoxia is most prevalent (Hinson et al.,



513 2021) will likely increase hypoxia more in the southern portion of the Bay. In addition, sea level
514 rise has also been found to preferentially increase hypoxia south of 38.5°N (Cai et al., 2021).

515 Our findings are focused on Chesapeake Bay hypoxia, but some lessons can also be drawn
516 from other coastal ecosystems where changes in watershed discharge and nutrient loadings are
517 also projected. In the Baltic Sea, Meier et al. (2011b) reported that hypoxia was very likely to
518 increase regardless of ESM or climate scenario, assuming targeted reductions in accordance with
519 the Baltic Sea Action Plan (decrease of nitrogen loads by $23 \pm 5\%$) were not met. Extensive
520 studies of projected oxygen change in the Baltic Sea have repeatedly demonstrated that climate
521 impacts are likely to increase hypoxic area (BACC II, 2015 and references therein), but more
522 recent reports (Saraiva et al., 2019a; Wählström et al., 2020; Meier et al., 2021, 2022) have
523 reaffirmed that nutrient reductions in accordance with the Baltic Sea Plan are also highly likely
524 to mitigate a substantial amount of those hypoxia increases. Repeated investigations into the
525 impact of increased discharge and higher temperatures in the Gulf of Mexico demonstrate a
526 likely expansion of hypoxic area (Justić et al. 1996; Lehrter et al., 2017; Laurent et al., 2018),
527 and additional nutrient reductions required to mitigate these impacts (Justić et al., 2003). Finally,
528 Whitney and Vlahos (2021) demonstrated a considerable erosion in oxygen gains due to nutrient
529 reductions in the presence of climate effects, reducing projected mid-century improvements by
530 14%, similar to the 9% increase in hypoxic volume reported by Irby et al. (2018) for O_2 levels <
531 2 mg L^{-1} . Although these studies include direct climate change impacts on coastal water bodies,
532 most support the findings here demonstrating that increases in discharge and associated nutrient
533 loadings are likely to increase Chesapeake Bay hypoxia. Overall, climate impacts on land have
534 the potential to profoundly modify biogeochemical interactions in the coastal zone and limit the
535 efficacy of nutrient reductions.

536

537 **4.2 Uncertainty in Climate Scenario Projections**

538

539 Projected changes in watershed discharge and nutrient delivery to the Chesapeake Bay
540 produce modest increases in estuarine hypoxia, with medium confidence (Mastrandrea et al.,
541 2010). AHV has a high degree of interannual variability, and future hypoxia estimates can be
542 modified substantially by the choice of ESM, downscaling method, and watershed model (Fig.
543 6c). While certain factors (particularly ESM and greenhouse gas emissions scenarios; Meier et
544 al., 2021) have previously been extensively evaluated in coastal systems with regards to hypoxia,
545 the results presented here also demonstrate the importance of terrestrial forcings on estuarine
546 oxygen levels.

547 In this study, future changes in watershed discharge, nitrogen loadings, and estuarine hypoxia
548 are found to be highly dependent on the selection of a specific ESM (Fig. 12), comprising a
549 majority of the total uncertainty in watershed outcomes and the greatest fraction of total
550 uncertainty for O_2 levels. When only the effect of ESM choice is considered (and downscaling
551 and hydrological model options are not; Fig. 10), the average projected change in AHV using
552 only three ESMs (often chosen to represent cool, median, and hot scenarios) has a greater
553 standard error than the selection of five in this study. Directly comparing results from the
554 experiment that compared five ESMs, two downscaling methods, and two watershed models
555 (Multi-Factor) versus that which only considered the impact of multiple ESMs (All ESMs)
556 shows a substantial overlap in the range of projected Δ AHV. In addition, multiple ESMs
557 downscaled with a single methodology and applied to one hydrological model produced
558 meaningfully different estimates of Δ AHV than a more balanced approach (Fig. 11).



559 Inter-model variability among ESMs appears to contribute most substantially to differences
560 in Bay watershed inputs, but the choice of downscaling methodology can also affect these
561 projections. The BCSD (Wood et al., 2004) and MACA (Abatzoglou and Brown, 2012)
562 downscaling methodologies used here employ different approaches to reduce historical ESM
563 biases, impacting the variability of spatio-temporal watershed hydrologic and water quality
564 responses. The ability to statistically downscale ESMs accurately depends on the spatially
565 coarser ESM's ability to simulate synoptic-scale (~1000 km) patterns and may still
566 underestimate the distributional tails of changes to temperature and precipitation. This increases
567 the importance of properly selecting a subset of ESMs (Abatzoglou and Brown, 2012).

568 Watershed model variability is caused by differences in the representation of processes that
569 affect discharge, those controlling the fate and transport of nutrients from land and in rivers, and
570 lag times of groundwater transport. The two watershed models used here project substantially
571 different results in watershed discharge and nitrogen delivery, even when the same changes to
572 meteorological forcings are applied (Fig. 6). DLEM projects no change or decreases in discharge
573 for nearly all scenarios, as opposed to greater average increases in discharge for Phase 6
574 scenarios (Fig. 6a), likely driven by differences in the representation of evapotranspiration.
575 Explicit soil biogeochemical processes within DLEM increase nitrification rates in warmer
576 climate scenarios, producing higher nitrate loadings than Phase 6 despite comparable discharge
577 changes (Fig. 6b). The greater total nitrogen loadings produced by Phase 6 are largely a
578 consequence of its parameterizations for erosion and refractory nitrogen bound to sediment.
579 Increases in bioavailable nitrate loadings, unlike refractory organic nitrogen that comprises the
580 majority of DON loadings, produce greater levels of primary production and remineralization
581 within the estuary. This largely explains the discrepancy between watershed model hypoxia
582 estimates (Table 5).

583 Our findings demonstrate the importance of considering differences among these three
584 factors (ESM, downscaling, and watershed model) that may contribute to a wider range of target
585 water quality variables and living resource responses in coastal marine ecosystems like the
586 Chesapeake Bay that are highly influenced by watershed processes. Hydrological model
587 assumptions can have potentially significant impacts on estuarine hypoxia. For example, the
588 relatively high organic nitrogen loadings in Phase 6 compared to DLEM's comparatively modest
589 exports under the same future scenarios result in different levels of annual hypoxia. While
590 dramatic increases in organic nitrogen loadings within Bay tributaries are mostly limited to
591 Cool/Wet Phase 6 scenarios, there is precedent for catastrophic erosion within the Bay watershed
592 driven by extreme precipitation events (Springer et al., 2001). The relative uncertainty
593 introduced by individual factors is also not necessarily equivalent for discharge, nitrogen
594 loadings, and AHV (Fig. 12). The complex connections between terrestrial runoff and
595 biogeochemical changes in the marine environment may expand further when higher order
596 trophic-level species are considered, and even more so when direct atmospheric impacts on the
597 Bay are also included. It is unlikely that general conclusions regarding the relative impacts of
598 different factors can be drawn for a marine ecosystem when only uncertainties in watershed
599 discharge and nutrient loadings are considered. Had our results only accounted for the impacts of
600 these factors on watershed changes and not estuarine oxygen levels, the role of downscaling
601 could be incorrectly assumed to contribute negligible variability to hypoxic volume (Fig. 12). It
602 is the complex interactions of nitrogen species transformations within this estuarine model that
603 are responsible for this somewhat unexpected large contribution of downscaling method
604 uncertainty that is less prominent in watershed changes.



605 Despite the relatively small magnitude of Chesapeake Bay watershed climate impacts on
606 estuarine hypoxia compared to previous evaluations of other climate impacts, like atmospheric
607 warming over the Bay (Irby et al., 2018; Ni et al., 2019; Tian et al., 2021), the relative
608 contributions of ESM and downscaling effects to the total uncertainty are large and are also
609 likely to expand the range of outcomes for other climate sensitivity studies in this region. This
610 suggests that, when attempting to determine a likely range of ecosystem outcomes, selecting
611 additional downscaling techniques and hydrological model responses should be considered in
612 addition to the more common practice of only selecting multiple ESMs.

613

614 **4.3 Hypoxia Lessened by Impacts of Management Actions**

615

616 Projections of changes to watershed discharge and nutrient delivery can better inform
617 regional environmental managers tasked with managing interactions among nutrient reduction
618 strategies, climate change, and coastal hypoxia (Hood et al., 2021; BACC II, 2015; Fennel and
619 Laurent, 2018). The Chesapeake Bay results provided in this analysis demonstrate that the
620 management actions mandated to improve water quality (USEPA, 2010) will decrease hypoxia
621 by roughly 50%, approximately an order of magnitude more than projected increases due only to
622 watershed climate change (Fig. 11). Therefore, nutrient reduction strategies are very likely to
623 remain effective at reducing watershed nutrient loading and its contribution to eutrophication and
624 hypoxia over a range of possible ESM scenarios (Mastrandrea et al., 2010). Should all
625 management actions be implemented as outlined in the USEPA's Total Maximum Daily Load
626 (USEPA, 2010), it is very likely that future climate impacts on Bay watershed runoff will worsen
627 Bay hypoxia by a far smaller amount, relative to 1990s reference conditions. These findings are
628 consistent with those of Irby et al. (2018) who also examined the impacts of watershed climate
629 on Chesapeake Bay hypoxia for the mid-21st century. When evaluating the effects of watershed
630 climate impacts and management actions together, Irby et al. (2018) estimated an average AHV
631 increase of 12.8 km³ d, which is well within the range of 17.1 ± 34.8 km³ d reported here.
632 (Interestingly, the combined impact of all climate stressors, i.e. atmosphere, ocean, and
633 watershed, increased average AHV by 24.5 km³ d, which is also within the range of the results
634 reported here). Because climate change impacts are likely to increase total nitrogen loads,
635 implementing nutrient reductions that do not account for the detrimental effects of climate
636 change will reduce the likelihood of attaining water quality targets. Further quantifying a range
637 of future estimates of watershed discharge and nitrogen loading using regional models is critical
638 to understanding the possibilities and limitations of mitigating negative climate impacts via
639 nutrient reductions.

640

641 Recent findings support the hypothesis that nutrient reductions will improve water quality
642 despite projected climate impacts in both freshwater systems (Wade et al., 2022) and other
643 coastal marine systems (Whitney and Vlahos, 2021; Saraiva et al., 2019a; Wählström et al.,
644 2020; Meier et al., 2021; Große et al., 2020; Jarvis et al., 2022). In the Chesapeake Bay, reduced
645 nutrient loading (Zhang et al., 2018; Murphy et al., 2022) has already helped mitigate growing
646 climate change pressures (Frankel et al., 2022), despite rapidly increasing Bay temperatures over
647 the past 30 years (Hinson et al., 2021). Like these prior studies, our findings confirm that
648 management actions will likely produce even greater benefits to O₂ in coastal zones strongly
649 affected by terrestrial runoff. While direct effects (e.g., air temperature) are expected to increase
hypoxia more so than watershed changes in Chesapeake Bay (Irby et al., 2018, Ni et al., 2019),



650 the comparatively greater impacts of management actions reported here are also likely to
651 substantially reduce the overall risk from a multitude of co-occurring climatic stressors.

652

653 **4.4 Study Limitations and Future Research Directions**

654

655 Despite the plainly evident finding of nutrient reduction strategies improving water quality
656 and counteracting negative climate change watershed impacts, a number of important caveats
657 should temper this conclusion. First, the subset of scenarios that include management actions is
658 limited to a set of five ESMS statistically downscaled with a single methodology and applied to
659 one watershed model. As demonstrated in this work, this assumption may oversimplify the
660 complex relationship between climate forcings and watershed model simulations, especially
661 given that DLEM scenarios produce more change in nitrate and consequently more hypoxia than
662 Phase 6 scenarios. Management actions implemented in Phase 6 nutrient reduction scenarios
663 represent a multitude of possible methods to reduce point and nonpoint source pollution that are
664 assumed to be fully implemented with a high operational efficacy by mid-century, but the true
665 performance of best management practices operating under future hydroclimatic stressors
666 remains largely unresolved (Hanson et al., 2022). Additionally, the importance of legacy
667 nitrogen inputs to the Bay may grow over time (Ator and Denver, 2015; Chang et al., 2021), and
668 can only be properly accounted for via a long-term transient simulation that accounts for
669 changing groundwater conditions.

670 A key strength of the delta method applied here is its ability to remove the influence of
671 interannual variability, which is known to strongly influence hypoxia in the Chesapeake Bay
672 (Bever et al., 2013). However, the delta method is unable to account for the impacts of
673 unanticipated extreme events, or changing patterns of precipitation intensity, duration, and
674 frequency that produce dramatic responses in sediment washoff, scour, and consequent
675 watershed organic nitrogen export. Air temperature and precipitation were the only watershed
676 model input variables adjusted in this analysis, allowing for a more equivalent comparison
677 between downscaling approaches. Future representations of watershed change may also better
678 account for changes in runoff through the inclusion of factors like ESM-estimated relative
679 humidity that can help avoid possible unreasonable amplification of potential evapotranspiration
680 that would decrease tributary discharge (Milly and Dunne, 2011) and associated nutrient loads.

681 Although main stem Bay oxygen levels are the focus of this study, watershed impacts are
682 also likely to influence water quality in smaller scale tributaries. Differences in Chesapeake Bay
683 temperatures introduced by ESM and downscaling method have also been investigated by
684 Muhling et al. (2018), and contribute to biogeochemical variability via direct impacts of
685 atmospheric temperature on Bay warming. Incorporating different facets of these relative
686 uncertainties into projections of coastal change has also been demonstrated to affect ecological
687 outcomes like those surrounding fisheries (Reum et al., 2020; Bossier et al., 2021). Thus, the
688 impacts of these uncertainties are also very likely to affect socio-economic systems tied to
689 coastal resources. The analytical method applied here is well established within climatic and
690 terrestrial settings, so the relative dearth of coastal applications (excluding Meier et al., 2021)
691 may be more related to a consequence of computational demand or greater focus on uncertain
692 parameterizations of marine biogeochemical processes (Jarvis et al., 2022) that also play a large
693 role in potential future hypoxia outcomes.

694

695 **5 Conclusions**



696

697

698

699

700

701

702

703

704

705

706

707

708

709

710

711

712

713

714

715

716

717

Coastal ecosystems like the Chesapeake Bay that are currently and will likely continue to be negatively affected by climate impacts exhibit complex responses in future scenarios, demonstrating our lack of complete system understanding. While this research reaffirms the importance of management actions in reducing levels of hypoxia, it also highlights the fact that uncertainties in climate-impacted watershed conditions will affect estimates of Chesapeake Bay O₂ levels. Additional study of uncertainty interactions within a full climate scenario (that includes the impacts of changing atmospheric and oceanic conditions) will help better quantify a range of hypoxia projections, among other environmental conditions within the Chesapeake Bay. These results underscore the need for additional rigorous analyses of model parameterizations and their contributions to model scenario uncertainty to help identify biogeochemical processes that are most sensitive to climate change impacts and warrant further investigation. The development of more rapid techniques to evaluate a broader range of future water quality and ecological outcomes, and an inspection of their underlying assumptions, can help provide a better mechanistic understanding of complex reactions to multiple climate stressors. Like ongoing efforts to reduce greenhouse gas emissions and lessen the impacts of future climate change globally, continuing efforts to reduce eutrophication in coastal waters will help improve ecosystem resilience and the benefits derived by communities dependent on their function. Indeed, nutrient reduction plans are likely to become even more essential to managers tasked with preserving the health and function of rapidly evolving coastal environments and unfamiliar future conditions.



718 **Appendix A:**

719

720

721

722

723

724

725

726

727

728

729

730

731

732

733

734

735

736

737

738

739

Original partitioning of organic nitrogen pools from the DLEM and Phase 6 watershed models was based on fixed fractions previously described in Frankel et al. (2022). There, 80% of the refractory organic nitrogen (rorN) loadings from Phase 6 were allocated to the small detritus nitrogen (SDeN) pool and the remainder was applied to the refractory dissolved organic nitrogen (rDON) pool in ChesROMS-ECB. More realistic changes to this partitioning of watershed rorN loadings were implemented, which decreased the lability of organic nitrogen loads overall. A specified threshold of rorN loadings was set at the 90th percentile of reference Phase 6 watershed inputs to the estuarine model, and thresholds were also set for individual river levels of discharge at the 50th and 90th percentiles of Phase 6 reference simulations. Below the 50th percentile of discharge levels, 80% of the rorN inputs below the specified rorN threshold were allocated to ChesROMS-ECB's SDeN pool, and the remainder were assigned to the rDON pool. Between the 50th and 90th percentiles of discharge events, 50% of the rorN load below the specified rorN threshold was apportioned to ChesROMS-ECB's SDeN and rDON pools. At the uppermost levels of discharge (greater than the 90th percentile), 5% of rorN was allocated to SDeN and 95% was given to rDON within ChesROMS-ECB. For any partitioning of an organic nitrogen load, regardless of the level of discharge, rorN loading above this cutoff was allocated to ChesROMS-ECB's rDON pool. The rorN load below this threshold was allocated according to the fractionations described above. Changes to Phase 6 watershed loadings were mapped to equivalent DLEM watershed input variables, following the methodology of Frankel et al. (2022).



740 **Competing Interests:** The authors declare that they have no conflict of interest.

741

742 **Author contribution:** MF, RN, HT, and GS were responsible for project conceptualization and
743 funding acquisition. MH, ZB, and GB were responsible for data curation used in the
744 experiments. KH and MF planned the model experiments; KH, MF, and PS are responsible for
745 the methodology (model creation). KH conducted the investigation and formal analysis, and
746 created software and visualizations of results; KH wrote the original manuscript draft; MF, RN,
747 MH, ZB, GB, PS, HT, and GS reviewed and edited the manuscript.

748

749 **Acknowledgements:** This paper is the result of research funded by the National Oceanic and
750 Atmospheric Administration's National Centers for Coastal Ocean Science under award
751 NA16NOS4780207 to the Virginia Institute of Marine Science. Additional funding support was
752 provided by the VIMS Academic Studies Office. Feedback from principal investigators, team
753 members, and the Management Transition and Advisory Group (MTAG) of the Chesapeake
754 Hypoxia Analysis & Modeling Program (CHAMP) benefited this research. The authors
755 acknowledge William & Mary Research Computing for providing computational resources
756 and/or technical support that have contributed to the results reported within this paper
757 (<https://www.wm.edu/it/rc>). The authors also acknowledge the World Climate Research
758 Programme's Working Group on Coupled Modelling, which is responsible for CMIP, and we
759 thank the climate modeling groups (listed in Table S3 of this paper) for producing and making
760 available their model output. For CMIP, the U.S. Department of Energy's Program for Climate
761 Model Diagnosis and Intercomparison provides coordinating support and led development of
762 software infrastructure in partnership with the Global Organization for Earth System Science
763 Portals. The model results used in the manuscript are permanently archived at the W&M
764 ScholarWorks data repository associated with this article and are available for free download
765 (<https://doi.org/xxxx>).



766 **References**

767

768 Abatzoglou, J. T., & Brown, T. J.: A comparison of statistical downscaling methods suited for
769 wildfire applications, *Int. J. Climatol.*, 32, 5, 772–780, <https://doi.org/10.1002/joc.2312>,
770 2012.

771 Anandhi, A., Frei, A., Pierson, D. C., Schneiderman, E. M., Zion, M. S., Lounsbury, D., &
772 Matonse, A. H.: Examination of change factor methodologies for climate change impact
773 assessment, *Water Resour. Res.*, 47, 3, 1–10, <https://doi.org/10.1029/2010WR009104>, 2011.

774 Ator, S.W., and Denver, J.M.: Understanding nutrients in the Chesapeake Bay watershed and
775 implications for management and restoration—the Eastern Shore (ver. 1.2, June 2015): U.S.
776 Geological Survey Circular 1406, 72 p., <http://dx.doi.org/10.3133/cir1406>, 2015.

777 Ator, S., Schwarz, G. E., Sekellick, A. J., & Bhatt, G.: Predicting Near-Term Effects of Climate
778 Change on Nitrogen Transport to Chesapeake Bay, *J. Am. Water Resour. Assoc.*, 58, 4, 578–
779 596, <https://doi.org/10.1111/1752-1688.13017>, 2022.

780 BACC II Author Team: Second Assessment of Climate Change for the Baltic Sea Basin, in:
781 Regional Climate Studies, Springer International Publishing, Cham,
782 <https://doi.org/10.1007/978-3-319-16006-1>, 2015.

783 Bevacqua, E., Shepherd, T. G., Watson, P. A. G., Sparrow, S., Wallom, D., & Mitchell, D.:
784 Larger Spatial Footprint of Wintertime Total Precipitation Extremes in a Warmer Climate,
785 *Geophys. Res. Lett.*, 48, 8, <https://doi.org/10.1029/2020GL091990>, 2021.

786 Bever, A. J., Friedrichs, M. A. M., Friedrichs, C. T., Scully, M. E., & Lanerolle, L. W. J.:
787 Combining observations and numerical model results to improve estimates of hypoxic
788 volume within the Chesapeake Bay, USA, *J. Geophys. Res. Ocean.*, 118, 10, 4924–4944,
789 <https://doi.org/10.1002/jgrc.20331>, 2013.

790 Bever, A. J., Friedrichs, M. A. M., Friedrichs, C. T., & Scully, M. E.: Estimating Hypoxic
791 Volume in the Chesapeake Bay Using Two Continuously Sampled Oxygen Profiles, *J.*
792 *Geophys. Res. Ocean.*, 123, 9, 6392–6407, <https://doi.org/10.1029/2018JC014129>, 2018.

793 Bever, A. J., Friedrichs, M. A. M., & St-Laurent, P.: Real-time environmental forecasts of the
794 Chesapeake Bay: Model setup, improvements, and online visualization, *Environ. Model.*
795 *Softw.*, 140, March, <https://doi.org/10.1016/j.envsoft.2021.105036>, 2021.

796 Bosshard, T., Carambia, M., Goergen, K., Kotlarski, S., Krahe, P., Zappa, M., & Schär, C.:
797 Quantifying uncertainty sources in an ensemble of hydrological climate-impact projections,
798 *Water Resour. Res.*, 49, 3, 1523–1536, <https://doi.org/10.1029/2011WR011533>, 2013.

799 Bossier, S., Nielsen, J. R., Almroth-Rosell, E., Höglund, A., Bastardie, F., Neuenfeldt, S.,
800 Wählström, I., & Christensen, A.: Integrated ecosystem impacts of climate change and
801 eutrophication on main Baltic fishery resources, *Ecol. Modell.*, 453, May,
802 <https://doi.org/10.1016/j.ecolmodel.2021.109609>, 2021.

803 Breitburg, D., Levin, L. A., Oschlies, A., Grégoire, M., Chavez, F. P., Conley, D. J., Garçon, V.,
804 Gilbert, D., Gutiérrez, D., Isensee, K., Jacinto, G. S., Limburg, K. E., Montes, I., Naqvi, S.
805 W. A., Pitcher, G. C., Rabalais, N. N., Roman, M. R., Rose, K. A., Seibel, B. A., ... Zhang,
806 J.: Declining oxygen in the global ocean and coastal waters, *Science (80-.)*, 359, 6371,
807 <https://doi.org/10.1126/science.aam7240>, 2018.

808 C3S (Copernicus Climate Change Service): “ERA5: Fifth Generation of ECMWF Atmospheric
809 Reanalyses of the Global Climate.” Copernicus Climate Change Service Climate Data Store
810 (CDS). <https://cds.climate.copernicus.eu/cdsapp#!/home>, 2017.



- 811 Cai, X., Shen, J., Zhang, Y. J., Qin, Q., Wang, Z., & Wang, H.: Impacts of Sea-Level Rise on
812 Hypoxia and Phytoplankton Production in Chesapeake Bay: Model Prediction and
813 Assessment, *J. Am. Water Resour. Assoc.*, 1–18, <https://doi.org/10.1111/1752-1688.12921>,
814 2021.
- 815 Carter, T.R., Parry, M.L., Nishioka, S. and Harasawa, H., 1994. Technical Guidelines for
816 Assessing Climate Change Impacts and Adaptations. Intergovernmental Panel on Climate
817 Change Working Group II. University College London and Center for Global Environmental
818 Research, Japan. 60 pp.
- 819 Chang, S. Y., Zhang, Q., Byrnes, D. K., Basu, N. B., & van Meter, K. J.: Chesapeake legacies:
820 The importance of legacy nitrogen to improving Chesapeake Bay water quality, *Environ.*
821 *Res. Lett.*, 16, 8, <https://doi.org/10.1088/1748-9326/ac0d7b>, 2021.
- 822 Chesapeake Bay Program DataHub: <http://data.chesapeakebay.net/WaterQuality>, last access: 18
823 April 2022.
- 824 Chesapeake Bay Program. Chesapeake Assessment and Scenario Tool (CAST) Version 2019.
825 Chesapeake Bay Program Office, <https://cast.chesapeakebay.net/>, 2020.
- 826 Da, F., Friedrichs, M. A. M., St-Laurent, P., Shadwick, E. H., Najjar, R. G., & Hinson, K. E.:
827 Mechanisms Driving Decadal Changes in the Carbonate System of a Coastal Plain Estuary, *J.*
828 *Geophys. Res. Ocean.*, 126, 6, 1–23, <https://doi.org/10.1029/2021JC017239>, 2021.
- 829 Dussin, R., Curchitser, E. N., Stock, C. A., & Van Oostende, N.: Biogeochemical drivers of
830 changing hypoxia in the California Current Ecosystem, *Deep. Res. Part II Top. Stud.*
831 *Oceanogr.*, 169–170, May, 104590, <https://doi.org/10.1016/j.dsr2.2019.05.013>, 2019.
- 832 Easton, Z., Scavia, D., Alexander, R., Band, L., Boomer, K., Kleinman, P., Martin, J., Miller, A.,
833 Pizzuto, J., Smith, D., Welty, C., Easton, Z., Scavia, D., Alexander, R., Band, L., Boomer,
834 K., Kleinman, P., Martin, J., & Miller, A.: Scientific and Technical Advisory Committee
835 Chesapeake Bay Watershed Model Phase 6 Review STAC Review Report (Vol. 47, Issue
836 September), 2017.
- 837 Feng, Y., Friedrichs, M. A. M., Wilkin, J., Tian, H., Yang, Q., Hofmann, E. E., Wiggert, J. D., &
838 Hood, R. R.: Chesapeake Bay nitrogen fluxes derived from a land- estuarine ocean
839 biogeochemical modeling system: Model description, evaluation, and nitrogen budgets, *J.*
840 *Geophys. Res. Biogeosciences*, 120, 1666–1695, <https://doi.org/10.1002/2017JG003800>,
841 2015.
- 842 Fennel, K., & Laurent, A.: N and P as ultimate and proximate limiting nutrients in the northern
843 Gulf of Mexico: Implications for hypoxia reduction strategies, *Biogeosciences*, 15, 10, 3121–
844 3131, <https://doi.org/10.5194/bg-15-3121-2018>, 2018.
- 845 Fennel, K., Gehlen, M., Brasseur, P., Brown, C. W., Ciavatta, S., Cossarini, G., Crise, A.,
846 Edwards, C. A., Ford, D., Friedrichs, M. A. M., Gregoire, M., Jones, E., Kim, H.-C.,
847 Lamouroux, J., Murtugudde, R., Perruche, C., and the GODAE OceanView Marine
848 Ecosystem Analysis and Prediction Task Team: Advancing Marine Biogeochemical and
849 Ecosystem Reanalyses and Forecasts as Tools for Monitoring and Managing Ecosystem
850 Health, *Front. Mar. Sci.*, 6, <https://doi.org/10.3389/fmars.2019.00089>, 2019.
- 851 Frankel, L. T., Friedrichs, M. A. M., St-Laurent, P., Bever, A. J., Lipcius, R. N., Bhatt, G., &
852 Shenk, G. W.: Nitrogen reductions have decreased hypoxia in the Chesapeake Bay: Evidence
853 from empirical and numerical modeling, *Sci. Total Environ.*, 814,
854 <https://doi.org/10.1016/j.scitotenv.2021.152722>, 2022.



- 855 Gilbert, D., Rabalais, N. N., Díaz, R. J., & Zhang, J.: Evidence for greater oxygen decline rates
856 in the coastal ocean than in the open ocean, *Biogeosciences*, 7, 7, 2283–2296,
857 <https://doi.org/10.5194/bg-7-2283-2010>, 2010.
- 858 Große, F., Fennel, K., Zhang, H., & Laurent, A.: Quantifying the contributions of riverine vs.
859 oceanic nitrogen to hypoxia in the East China Sea, *Biogeosciences*, 17, 10, 2701–2714,
860 <https://doi.org/10.5194/bg-17-2701-2020>, 2020.
- 861 Gudmundsson, L., Boulange, J., Do, H. X., Gosling, S. N., Grillakis, M. G., Koutroulis, A. G.,
862 Leonard, M., Liu, J., Schmied, H. M., Papadimitriou, L., Pokhrel, Y., Seneviratne, S. I.,
863 Satoh, Y., Thiery, W., Westra, S., Zhang, X., & Zhao, F.: Globally observed trends in mean
864 and extreme river flow attributed to climate change, *Science*, 371, 6534, 1159–1162,
865 <https://doi.org/10.1126/science.aba3996>, 2021.
- 866 Hagy, J. D., Boynton, W. R., Keefe, C. W., & Wood, K. V.: Hypoxia in Chesapeake Bay, 1950–
867 2001: Long-term change in relation to nutrient loading and river flow, *Estuaries*, 27, 4, 634–
868 658, <https://doi.org/10.1007/BF02907650>, 2004.
- 869 Hanson, J., E. Bock, B. Asfaw, and Z.M. Easton.: A systematic review of Chesapeake Bay
870 climate change impacts and uncertainty: watershed processes, pollutant delivery and BMP
871 performance. CBP/TRS-330-22. Available at <https://bit.ly/BMP-CC-synth>, 2022.
- 872 Harding, L. W., Mallonee, M. E., & Perry, E. S.: Toward a predictive understanding of primary
873 productivity in a temperate, partially stratified estuary, *Estuar. Coast. Shelf Sci.*, 55, 3, 437–
874 463, <https://doi.org/10.1006/ecss.2001.0917>, 2002.
- 875 Hawkins, E., & Sutton, R.: The potential to narrow uncertainty in regional climate predictions,
876 *Bull. Am. Meteorol. Soc.*, 90, 8, 1095–1107, <https://doi.org/10.1175/2009BAMS2607.1>,
877 2009.
- 878 Hein, B., Viergutz, C., Wyrwa, J., Kirchesch, V., & Schöl, A.: Impacts of climate change on the
879 water quality of the Elbe Estuary (Germany), *J. Appl. Water Eng. Res.*, 6, 1, 28–39,
880 <https://doi.org/10.1080/23249676.2016.1209438>, 2018.
- 881 Hinson, K. E., Friedrichs, M. A. M., St-Laurent, P., Da, F., & Najjar, R. G.: Extent and Causes of
882 Chesapeake Bay Warming, *J. Am. Water Resour. Assoc.*, 1–21,
883 <https://doi.org/10.1111/1752-1688.12916>, 2021.
- 884 Hirsch, R. M., Moyer, D. L., & Archfield, S. A.: Weighted regressions on time, discharge, and
885 season (WRTDS), with an application to chesapeake bay river inputs, *J. Am. Water Resour.*
886 *Assoc.*, 46, 5, 857–880, <https://doi.org/10.1111/j.1752-1688.2010.00482.x>, 2010.
- 887 Hong, B., Liu, Z., Shen, J., Wu, H., Gong, W., Xu, H., & Wang, D.: Potential physical impacts
888 of sea-level rise on the Pearl River Estuary, China, *J. Mar. Syst.*, 201,
889 <https://doi.org/10.1016/j.jmarsys.2019.103245>, 2020.
- 890 Hood, R. R., Shenk, G. W., Dixon, R. L., Smith, S. M. C., Ball, W. P., Bash, J. O., Batiuk, R.,
891 Boomer, K., Brady, D. C., Cerco, C., Claggett, P., de Mutsert, K., Easton, Z. M., Elmore, A.
892 J., Friedrichs, M. A. M., Harris, L. A., Ihde, T. F., Lacher, L., Li, L., ... Zhang, Y. J.: The
893 Chesapeake Bay program modeling system: Overview and recommendations for future
894 development, *Ecol. Modell.*, 456, July, <https://doi.org/10.1016/j.ecolmodel.2021.109635>,
895 2021.
- 896 Howarth, R. W., Swaney, D. P., Boyer, E. W., Marino, R., Jaworski, N., & Goodale, C.: The
897 influence of climate on average nitrogen export from large watersheds in the Northeastern
898 United States, *Biogeochemistry*, 79, 1–2, 163–186, <https://doi.org/10.1007/s10533-006-9010-1>,
899 2006.



- 900 Huang, H., Patricola, C. M., Winter, J. M., Osterberg, E. C., & Mankin, J. S.: Rise in Northeast
901 US extreme precipitation caused by Atlantic variability and climate change, *Weather Clim.*
902 *Extrem.*, 33, January, <https://doi.org/10.1016/j.wace.2021.100351>, 2021.
- 903 IPCC, 2013: *Climate Change 2013: The Physical Science Basis. Contribution of Working Group*
904 *I to the Fifth Assessment Report of the Intergovernmental Panel on Climate Change*
905 [Stocker, T.F., D. Qin, G.-K. Plattner, M. Tignor, S.K. Allen, J. Boschung, A. Nauels, Y.
906 Xia, V. Bex and P.M. Midgley (eds.)]. Cambridge University Press, Cambridge, United
907 Kingdom and New York, NY, USA, 1535 pp.
- 908 Irby, I. D., Friedrichs, M. A. M., Da, F., & Hinson, K. E.: The competing impacts of climate
909 change and nutrient reductions on dissolved oxygen in Chesapeake Bay, *Biogeosciences*, 15,
910 9, 2649–2668, <https://doi.org/10.5194/bg-15-2649-2018>, 2018.
- 911 Irby, I. D., Friedrichs, M. A. M., Friedrichs, C. T., Bever, A. J., Hood, R. R., Lanerolle, L. W. J.,
912 Scully, M. E., Sellner, K., Shen, J., Testa, J., Li, M., Wang, H., Wang, P., Linker, L., & Xia,
913 M.: Challenges associated with modeling low-oxygen waters in Chesapeake Bay: A multiple
914 model comparison, *Biogeosciences*, 13, 7, 2011–2028, [https://doi.org/10.5194/bgd-12-](https://doi.org/10.5194/bgd-12-20361-2015)
915 [20361-2015](https://doi.org/10.5194/bgd-12-20361-2015), 2016.
- 916 Jarvis, B. M., Pauer, J. J., Melendez, W., Wan, Y., Lehrter, J. C., Lowe, L. L., & Simmons, C.
917 W.: Inter-model comparison of simulated Gulf of Mexico hypoxia in response to reduced
918 nutrient loads: Effects of phytoplankton and organic matter parameterization, *Environ.*
919 *Model. Softw.*, 151, 105365, <https://doi.org/10.1016/j.envsoft.2022.105365>, 2022.
- 920 Justić, D., Bierman Jr, V. J., Scavia, D., & Hetland, R. D.: Forecasting Gulf's Hypoxia : The
921 Next 50 Years ? Forecasting Gulf's Hypoxia: The Next 50 Years ?, *Estuaries and Coasts*, 30,
922 5, 791–801, <https://doi.org/10.1007/BF02841334>, 2007.
- 923 Justić, D., Rabalais, N. N., & Turner, R. E.: Effects of climate change on hypoxia in coastal
924 waters: A doubled CO₂ scenario for the northern Gulf of Mexico, *Limnol. Oceanogr.*, 41, 5,
925 992–1003, <https://doi.org/10.4319/lo.1996.41.5.0992>, 1996.
- 926 Justić, D., Rabalais, N. N., & Turner, R. E.: Simulated responses of the Gulf of Mexico hypoxia
927 to variations in climate and anthropogenic nutrient loading, *J. Mar. Syst.*, 42, 3–4, 115–126,
928 [https://doi.org/10.1016/S0924-7963\(03\)00070-8](https://doi.org/10.1016/S0924-7963(03)00070-8), 2003.
- 929 Katsavounidis, I., Kuo, C. C. J., & Zhang, Z.: A New Initialization Technique for Generalized
930 Lloyd Iteration, *IEEE Signal Process. Lett.*, 1, 10, 144–146,
931 <https://doi.org/10.1109/97.329844>, 1994.
- 932 Kemp, W. M., Boynton, W. R., Adolf, J. E., Boesch, D. F., Boicourt, W. C., Brush, G.,
933 Cornwell, J. C., Fisher, T. R., Glibert, P. M., Hagy, J. D., Harding, L. W., Houde, E. D.,
934 Kimmel, D. G., Miller, W. D., Newell, R. I. E., Roman, M. R., Smith, E. M., & Stevenson, J.
935 C.: Eutrophication of Chesapeake Bay: Historical trends and ecological interactions, *Mar.*
936 *Ecol. Prog. Ser.*, 303, 1–29, <https://doi.org/10.3354/meps303001>, 2005.
- 937 Lachkar, Z., Lévy, M., & Smith, K. S.: Strong Intensification of the Arabian Sea Oxygen
938 Minimum Zone in Response to Arabian Gulf Warming, *Geophys. Res. Lett.*, 46, 10, 5420–
939 5429, <https://doi.org/10.1029/2018GL081631>, 2019.
- 940 Lajaunie-Salla, K., Sottolichio, A., Schmidt, S., Litrico, X., Binet, G., & Abril, G.: Future
941 intensification of summer hypoxia in the tidal Garonne River (SW France) simulated by a
942 coupled hydro sedimentary-biogeochemical model, *Environ. Sci. Pollut. Res.*, 25, 32, 31957–
943 31970, <https://doi.org/10.1007/s11356-018-3035-6>, 2018.



- 944 Laurent, A., Fennel, K., Ko, D. S., & Lehrter, J.: Climate change projected to exacerbate impacts
945 of coastal Eutrophication in the Northern Gulf of Mexico, *J. Geophys. Res. Ocean.*, 123, 5,
946 3408–3426, <https://doi.org/10.1002/2017JC013583>, 2018.
- 947 Lee, M., Shevliakova, E., Malyshev, S., Milly, P. C. D., & Jaffé, Peter, R.: Climate variability
948 and extremes, interacting with nitrogen storage, amplify eutrophication risk, *Geophys. Res.*
949 *Lett.*, 43, 7520–7528, <https://doi.org/10.1002/2016GL069254>, 2016.
- 950 Lehrter, J. C., Ko, D. S., Lowe, L. L., & Penta, B.: Predicted Effects of Climate Change on
951 Northern Gulf of Mexico Hypoxia, In D. Justić, K. A. Rose, R. D. Hetland, & K. Fennel
952 (Eds.), *Modeling Coastal Hypoxia: Numerical Simulations of Patterns, Controls and Effects*
953 *of Dissolved Oxygen Dynamics* (pp. 173–214) Springer [https://doi.org/10.1007/978-3-319-](https://doi.org/10.1007/978-3-319-54571-4_8)
954 [54571-4_8](https://doi.org/10.1007/978-3-319-54571-4_8), 2017.
- 955 Lomas, M. W., Glibert, P. M., Shiah, F. K., & Smith, E. M.: Microbial processes and
956 temperature in Chesapeake Bay: Current relationships and potential impacts of regional
957 warming, *Glob. Chang. Biol.*, 8, 1, 51–70, <https://doi.org/10.1046/j.1365-2486.2002.00454.x>,
958 2002.
- 959 MACAv2-METDATA: [https://data.nal.usda.gov/dataset/climate-data-rpa-2020-assessment-](https://data.nal.usda.gov/dataset/climate-data-rpa-2020-assessment-macav2-metdata-historical-modeled-1950-2005-and-future-2006-2099-projections-conterminous-united-states-124-degree-grid-scale)
960 [macav2-metdata-historical-modeled-1950-2005-and-future-2006-2099-projections-](https://data.nal.usda.gov/dataset/climate-data-rpa-2020-assessment-macav2-metdata-historical-modeled-1950-2005-and-future-2006-2099-projections-conterminous-united-states-124-degree-grid-scale)
961 [conterminous-united-states-124-degree-grid-scale](https://data.nal.usda.gov/dataset/climate-data-rpa-2020-assessment-macav2-metdata-historical-modeled-1950-2005-and-future-2006-2099-projections-conterminous-united-states-124-degree-grid-scale), last access: 25 April 2018.
- 962 Madakumbura, G. D., Goldenson, N., & Hall, A.: Over Global Land Areas Seen in Multiple
963 Observational Datasets, *Nat. Commun.* <http://dx.doi.org/10.1038/s41467-021-24262-x> 2021.
- 964 Mastrandrea, M.D., Field, C.B., Stocker, T.F., Edenhofer O., Ebi, K.L., Frame, D.J., Held H.,
965 Kriegler, E., Mach, K.J., Matschoss, P.R., Plattner, G.-K., Yohe, G.W., & Zwiers, F.W.:
966 Guidance Note for Lead Authors of the IPCC Fifth Assessment Report on Consistent
967 Treatment of Uncertainties. Intergovernmental Panel on Climate Change (IPCC). Available
968 at <http://www.ipcc.ch>, 2010.
- 969 Meier, H. E. M., Andersson, H. C., Eilola, K., Gustafsson, B. G., Kuznetsov, I., Miller-Karulis,
970 B., Neumann, T., & Savchuk, O. P.: Hypoxia in future climates: A model ensemble study for
971 the Baltic Sea, *Geophys. Res. Lett.*, 38, 24, 1–6, <https://doi.org/10.1029/2011GL049929>,
972 2011a.
- 973 Meier, H. E. M., Dieterich, C., & Gröger, M.: Natural variability is a large source of uncertainty
974 in future projections of hypoxia in the Baltic Sea, *Commun. Earth Environ.*, 2, 1,
975 <https://doi.org/10.1038/s43247-021-00115-9>, 2021.
- 976 Meier, H. E. M., Dieterich, C., Gröger, M., Dutheil, C., Börgel, F., Safonova, K., Christensen, O.
977 B., & Kjellström, E.: Oceanographic regional climate projections for the Baltic Sea until
978 2100, *Earth Syst. Dyn.*, 13, 159–199, <https://doi.org/10.5194/esd-13-159-2022>, 2022.
- 979 Meier, H. E. M., Edman, M., Eilola, K., Placke, M., Neumann, T., Andersson, H. C.,
980 Brunnabend, S. E., Dieterich, C., Frauen, C., Friedland, R., Gröger, M., Gustafsson, B. G.,
981 Gustafsson, E., Isaev, A., Kniebusch, M., Kuznetsov, I., Müller-Karulis, B., Naumann, M.,
982 Omstedt, A., ... Savchuk, O. P.: Assessment of uncertainties in scenario simulations of
983 biogeochemical cycles in the Baltic Sea, *Front. Mar. Sci.*, 6, MAR,
984 <https://doi.org/10.3389/fmars.2019.00046>, 2019.
- 985 Meier, H. E. M., Eilola, K., & Almroth, E.: Climate-related changes in marine ecosystems
986 simulated with a 3-dimensional coupled physical-biogeochemical model of the Baltic Sea,
987 *Clim. Res.*, 48, 1, 31–55, <https://doi.org/10.3354/cr00968>, 2011b.



- 988 Meire, L., Soetaert, K. E. R., & Meysman, F. J. R.: Impact of global change on coastal oxygen
989 dynamics and risk of hypoxia, *Biogeosciences*, 10, 4, 2633–2653, [https://doi.org/10.5194/bg-](https://doi.org/10.5194/bg-10-2633-2013)
990 10-2633-2013, 2013.
- 991 Milly, P. C. D., & Dunne, K. A.: On the hydrologic adjustment of climate-model projections:
992 The potential pitfall of potential evapotranspiration, *Earth Interact.*, 15, 1, 1–14,
993 <https://doi.org/10.1175/2010EI363.1>, 2011.
- 994 Muhling, B. A., Gaitán, C. F., Stock, C. A., Saba, V. S., Tommasi, D., & Dixon, K. W.: Potential
995 Salinity and Temperature Futures for the Chesapeake Bay Using a Statistical Downscaling
996 Spatial Disaggregation Framework, *Estuaries and Coasts*, 41, 2, 349–372,
997 <https://doi.org/10.1007/s12237-017-0280-8>, 2018.
- 998 Murphy, R. R., Keisman, J., Harcum, J., Karrh, R. R., Lane, M., Perry, E. S., & Zhang, Q.:
999 Nutrient Improvements in Chesapeake Bay: Direct Effect of Load Reductions and
1000 Implications for Coastal Management, *Environ. Sci. Technol.*, 56, 1, 260–270,
1001 <https://doi.org/10.1021/acs.est.1c05388>, 2022.
- 1002 Najjar, R. G., Pyke, C. R., Adams, M. B., Breitbart, D., Hershner, C., Kemp, M., Howarth, R.,
1003 Mulholland, M. R., Paolisso, M., Secor, D., Sellner, K., Wardrop, D., & Wood, R.: Potential
1004 climate-change impacts on the Chesapeake Bay, *Estuar. Coast. Shelf Sci.*, 86, 1, 1–20,
1005 <https://doi.org/10.1016/j.ecss.2009.09.026>, 2010.
- 1006 Nash, J. E., & Sutcliffe, J. V.: River Flow Forecasting through Conceptual Models Part I - A
1007 Discussion of Principles*, *J. Hydrol.*, 10, 282–290, 1970.
- 1008 Neumann, T., Eilola, K., Gustafsson, B., Müller-Karulis, B., Kuznetsov, I., Meier, H. E. M., &
1009 Savchuk, O. P.: Extremes of temperature, oxygen and blooms in the baltic sea in a changing
1010 climate, *Ambio*, 41, 6, 574–585, <https://doi.org/10.1007/s13280-012-0321-2>, 2012.
- 1011 Ni, W., Li, M., Ross, A. C., & Najjar, R. G.: Large Projected Decline in Dissolved Oxygen in a
1012 Eutrophic Estuary Due to Climate Change, *J. Geophys. Res. Ocean.*, 124, 11, 8271–8289,
1013 <https://doi.org/10.1029/2019JC015274>, 2019.
- 1014 Northrop, P. J., & Chandler, R. E.: Quantifying sources of uncertainty in projections of future
1015 climate, *J. Clim.*, 27, 23, 8793–8808, <https://doi.org/10.1175/JCLI-D-14-00265.1>, 2014.
- 1016 Officer, C. B., Biggs, R. B., Taft, J. L., Cronin, L. E., Tyler, M. A., & Boynton, W. R.:
1017 Chesapeake Bay anoxia: Origin, development, and significance, *Science*, 223, 4631, 22–27,
1018 <https://doi.org/10.1126/science.223.4631.22>, 1984.
- 1019 Ohn, I., Kim, S., Seo, S. B., Kim, Y. O., & Kim, Y.: Model-wise uncertainty decomposition in
1020 multi-model ensemble hydrological projections, *Stoch. Environ. Res. Risk Assess.*, 35, 12,
1021 2549–2565, <https://doi.org/10.1007/s00477-021-02039-4>, 2021.
- 1022 Olson, M.: Guide to Using Chesapeake Bay Program Water Quality Monitoring Data, edited by
1023 M. Mallonee and M.E. Ley. Annapolis, MD: Chesapeake Bay Program, 2012.
- 1024 Pan, S., Bian, Z., Tian, H., Yao, Y., Najjar, R. G., Friedrichs, M. A. M., Hofmann, E. E., Xu, R.,
1025 & Zhang, B.: Impacts of Multiple Environmental Changes on Long-Term Nitrogen Loading
1026 From the Chesapeake Bay Watershed, *J. Geophys. Res. Biogeosciences*, 126, 5,
1027 <https://doi.org/10.1029/2020JG005826>, 2021.
- 1028 Peterson, E. L.: Benthic shear stress and sediment condition, *Aquac. Eng.*, 21, 2, 85–111,
1029 [https://doi.org/10.1016/S0144-8609\(99\)00025-4](https://doi.org/10.1016/S0144-8609(99)00025-4), 1999.
- 1030 Pozo Buil, M., Jacox, M. G., Fiechter, J., Alexander, M. A., Bograd, S. J., Curchitser, E. N.,
1031 Edwards, C. A., Rykaczewski, R. R., & Stock, C. A.: A Dynamically Downscaled Ensemble
1032 of Future Projections for the California Current System, *Front. Mar. Sci.*, 8, April, 1–18,
1033 <https://doi.org/10.3389/fmars.2021.612874>, 2021.



- 1034 Prudhomme, C., Reynard, N., & Crooks, S.: Downscaling of global climate models for flood
1035 frequency analysis: Where are we now?, *Hydrol. Process.*, 16, 1137–1150,
1036 <https://doi.org/10.1002/hyp.1054>, 2002.
- 1037 Reum, J. C. P., Blanchard, J. L., Holsman, K. K., Aydin, K., Hollowed, A. B., Hermann, A. J.,
1038 Cheng, W., Faig, A., Haynie, A. C., & Punt, A. E.: Ensemble Projections of Future Climate
1039 Change Impacts on the Eastern Bering Sea Food Web Using a Multispecies Size Spectrum
1040 Model, *Front. Mar. Sci.*, 7, March, 1–17, <https://doi.org/10.3389/fmars.2020.00124>, 2020.
- 1041 Ross, A. C., & Najjar, R. G.: Evaluation of methods for selecting climate models to simulate
1042 future hydrological change, *Clim. Change*, 157, 3–4, 407–428,
1043 <https://doi.org/10.1007/s10584-019-02512-8>, 2019.
- 1044 Ryabchenko, V. A., Karlin, L. N., Isaev, A. V., Vankevich, R. E., Eremina, T. R., Molchanov,
1045 M. S., & Savchuk, O. P.: Model estimates of the eutrophication of the Baltic Sea in the
1046 contemporary and future climate, *Oceanology*, 56, 1, 36–45,
1047 <https://doi.org/10.1134/S0001437016010161>, 2016.
- 1048 Saraiva, S., Markus Meier, H. E., Andersson, H., Höglund, A., Dieterich, C., Gröger, M.,
1049 Hordoir, R., & Eilola, K.: Baltic Sea ecosystem response to various nutrient load scenarios in
1050 present and future climates, *Clim. Dyn.*, 52, 5–6, 3369–3387, [https://doi.org/10.1007/s00382-](https://doi.org/10.1007/s00382-018-4330-0)
1051 [018-4330-0](https://doi.org/10.1007/s00382-018-4330-0), 2019a.
- 1052 Saraiva, S., Markus Meier, H. E., Andersson, H., Höglund, A., Dieterich, C., Gröger, M.,
1053 Hordoir, R., & Eilola, K.: Uncertainties in projections of the Baltic Sea ecosystem driven by
1054 an ensemble of global climate models, *Front. Earth Sci.*, 6, January, 1–18,
1055 <https://doi.org/10.3389/feart.2018.00244>, 2019b.
- 1056 Schaefer, S. C., & Alber, M.: Temperature controls a latitudinal gradient in the proportion of
1057 watershed nitrogen exported to coastal ecosystems, *Biogeochemistry*, 85, 3, 333–346,
1058 <https://doi.org/10.1007/s10533-007-9144-9>, 2007.
- 1059 Shenk, G., M. Bennett, D. Boesch, L. Currey, M. Friedrichs, M. Herrmann, R. Hood, T. Johnson,
1060 L. Linker, A. Miller, and D. Montali. 2021a. Chesapeake Bay Program Climate Change
1061 Modeling 2.0 Workshop. STAC Publication Number 21-003, Edgewater, MD. 35 pp.
- 1062 Shenk, G. W., Bhatt, G., Tian, R., Cerco, C.F., Bertani, I., Linker, L.C., 2021b. Modeling
1063 Climate Change Effects on Chesapeake Water Quality Standards and Development of 2025
1064 Planning Targets to Address Climate Change. CBPO Publication Number 328-21, Annapolis,
1065 MD. 145 pp.
- 1066 Siedlecki, S. A., Pilcher, D., Howard, E. M., Deutsch, C., MacCready, P., Norton, E. L., Frenzel,
1067 H., Newton, J., Feely, R. A., Alin, S. R., & Klinger, T.: Coastal processes modify projections
1068 of some climate-driven stressors in the California Current System, *Biogeosciences*, 18, 9,
1069 2871–2890, <https://doi.org/10.5194/bg-18-2871-2021>, 2021.
- 1070 Sinha, E., Michalak, A. M., & Balaji, V.: Eutrophication will increase during the 21st century as
1071 a result of precipitation changes, *Science*, 357, 6349, 1–5,
1072 <https://doi.org/10.1126/science.aan2409>, 2017.
- 1073 Springer, G. S., Dowdy, H. S., & Eaton, L. S.: Sediment budgets for two mountainous basins
1074 affected by a catastrophic storm: Blue ridge mountains, Virginia, *Geomorphology*, 37, 1–2,
1075 135–148, [https://doi.org/10.1016/S0169-555X\(00\)00066-0](https://doi.org/10.1016/S0169-555X(00)00066-0), 2001.
- 1076 St-Laurent, P., Friedrichs, M. A. M., Najjar, R. G., Shadwick, E. H., Tian, H., & Yao, Y.:
1077 Relative impacts of global changes and regional watershed changes on the inorganic carbon
1078 balance of the Chesapeake Bay, *Biogeosciences*, 17, 14, 3779–3796,
1079 <https://doi.org/10.5194/bg-17-3779-2020>, 2020.



- 1080 Tango, P. J., & Batiuk, R. A.: Chesapeake Bay recovery and factors affecting trends: Long-term
1081 monitoring, indicators, and insights, *Reg. Stu. in Mar. Sci.*, 4, 12-20,
1082 <https://doi.org/10.1016/j.rsma.2015.11.010>, 2016.
- 1083 Tebaldi, C., Arblaster, J. M., & Knutti, R.: Mapping model agreement on future climate
1084 projections, *Geophys. Res. Lett.*, 38, 23, 1–5, <https://doi.org/10.1029/2011GL049863>, 2011.
- 1085 Testa, J. M., Basenback, N., Shen, C., Cole, K., Moore, A., Hodgkins, C., & Brady, D. C.:
1086 Modeling Impacts of Nutrient Loading, Warming, and Boundary Exchanges on Hypoxia and
1087 Metabolism in a Shallow Estuarine Ecosystem, *J. Am. Water Resour. Assoc.*, 1–22,
1088 <https://doi.org/10.1111/1752-1688.12912>, 2021.
- 1089 Testa, J. M., Murphy, R. R., Brady, D. C., & Kemp, W. M.: Nutrient-and climate-induced shifts
1090 in the phenology of linked biogeochemical cycles in a temperate estuary, *Front. Mar. Sci.*, 5,
1091 114, <https://doi.org/10.3389/fmars.2018.00114>, 2018.
- 1092 Tian, R., Cerco, C. F., Bhatt, G., Linker, L. C., & Shenk, G. W.: Mechanisms Controlling
1093 Climate Warming Impact on the Occurrence of Hypoxia in Chesapeake Bay, *J. Am. Water
1094 Resour. Assoc.*, 1–21, <https://doi.org/10.1111/1752-1688.12907>, 2021.
- 1095 USEPA (U.S. Environmental Protection Agency): Chesapeake Bay Total Maximum Daily Load
1096 for Nitrogen, Phosphorus and Sediment. Annapolis, MD: U.S. Environmental Protection
1097 Agency Chesapeake Bay Program Office. [http://www.epa.gov/
1098 reg3wapd/tmdl/ChesapeakeBay/tmdlexec.html](http://www.epa.gov/reg3wapd/tmdl/ChesapeakeBay/tmdlexec.html), 2010.
- 1099 Vetter, T., Reinhardt, J., Flörke, M., van Griensven, A., Hattermann, F., Huang, S., Koch, H.,
1100 Pechlivanidis, I. G., Plötner, S., Seidou, O., Su, B., Vervoort, R. W., & Krysanova, V.:
1101 Evaluation of sources of uncertainty in projected hydrological changes under climate change
1102 in 12 large-scale river basins, *Clim. Change*, 141, 3, 419–433,
1103 <https://doi.org/10.1007/s10584-016-1794-y>, 2017.
- 1104 Wade, A. J., Skeffington, R. A., Couture, R.-M., Erlandsson Lampa, M., Groot, S., Halliday, S.
1105 J., Harezlak, V., Hejzlar, J., Jackson-Blake, L. A., Lepistö, A., Papastergiadou, E., Riera, J.
1106 L., Rankinen, K., Shahgedanova, M., Trolle, D., Whitehead, P. G., Psaltopoulos, D., &
1107 Skuras, D.: Land Use Change to Reduce Freshwater Nitrogen and Phosphorus will Be
1108 Effective Even with Projected Climate Change, *Water*, 14, 5, 829,
1109 <https://doi.org/10.3390/w14050829>, 2022.
- 1110 Wagena, M. B., Collick, A. S., Ross, A. C., Najjar, R. G., Rau, B., Sommerlot, A. R., Fuka, D.
1111 R., Kleinman, P. J. A., & Easton, Z. M.: Impact of climate change and climate anomalies on
1112 hydrologic and biogeochemical processes in an agricultural catchment of the Chesapeake
1113 Bay watershed, USA, *Sci. Total Environ.*, 637–638, 1443–1454,
1114 <https://doi.org/10.1016/j.scitotenv.2018.05.116>, 2018.
- 1115 Wählström, I., Höglund, A., Almroth-Rosell, E., MacKenzie, B. R., Gröger, M., Eilola, K.,
1116 Plikshs, M., & Andersson, H. C.: Combined climate change and nutrient load impacts on
1117 future habitats and eutrophication indicators in a eutrophic coastal sea, *Limnol. Oceanogr.*,
1118 1–18, <https://doi.org/10.1002/lno.11446>, 2020.
- 1119 Wakelin, S. L., Artioli, Y., Holt, J. T., Butenschön, M., & Blackford, J.: Controls on near-bed
1120 oxygen concentration on the Northwest European Continental Shelf under a potential future
1121 climate scenario, *Prog. Oceanogr.*, 93, 2020.
- 1122 Wang, H. M., Chen, J., Xu, C. Y., Zhang, J., & Chen, H.: A Framework to Quantify the
1123 Uncertainty Contribution of GCMs Over Multiple Sources in Hydrological Impacts of
1124 Climate Change, *Earth's Futur.*, 8, 8, <https://doi.org/10.1029/2020EF001602>, 2020.



- 1125 Wang, P., Linker, L., Wang, H., Bhatt, G., Yactayo, G., Hinson, K.E., & Tian, R.: Assessing
1126 water quality of the Chesapeake Bay by the impact of sea level rise and warming, *IOP Conf.*
1127 *Ser. Earth Environ. Sci.*, 82, 1, <https://doi.org/10.1088/1755-1315/82/1/012001>, 2017.
- 1128 Whitney, M. M., & Vlahos, P.: Reducing Hypoxia in an Urban Estuary despite Climate
1129 Warming, *Environ. Sci. Technol.*, 55, 2, 941–951, <https://doi.org/10.1021/acs.est.0c03964>,
1130 2021.
- 1131 Whitney, M.M.: Observed and projected global warming pressure on coastal hypoxia,
1132 *Biogeosciences*, 19, 4479–4497, <https://doi.org/10.5194/bg-19-4479-2022>, 2022.
- 1133 Wolkovich, E. M., Cook, B. I., Allen, J. M., Crimmins, T. M., Betancourt, J. L., Travers, S. E.,
1134 Pau, S., Regetz, J., Davies, T. J., Kraft, N. J. B., Ault, T. R., Bolmgren, K., Mazer, S. J.,
1135 McCabe, G. J., McGill, B. J., Parmesan, C., Salamin, N., Schwartz, M. D., & Cleland, E. E.:
1136 Warming experiments underpredict plant phenological responses to climate change, *Nature*,
1137 485, 7399, 494–497, <https://doi.org/10.1038/nature11014>, 2012.
- 1138 Wood, A. W., Leung, L. R., Sridhar, V., & Lettenmaier, D. P.: Hydrologic implications of
1139 dynamical and statistical approaches to downscaling climate model outputs, *Clim. Change*,
1140 62, 1–3, 189–216, <https://doi.org/10.1023/B:CLIM.0000013685.99609.9e>, 2004.
- 1141 Yang, Q., Tian, H., Friedrichs, M. A. M., Liu, M., Li, X., & Yang, J.: Hydrological responses to
1142 climate and land-use changes along the north american east coast: A 110-Year historical
1143 reconstruction, *J. Am. Water Resour. Assoc.*, 51, 1, 47–67,
1144 <https://doi.org/10.1111/jawr.12232>, 2015.
- 1145 Yang, X., Wang, X., Cai, Z., & Cao, W.: Detecting spatiotemporal variations of maximum
1146 rainfall intensities at various time intervals across Virginia in the past half century, *Atmos.*
1147 *Res.*, 255, <https://doi.org/10.1016/j.atmosres.2021.105534>, 2021.
- 1148 Yao, Y., Tian, H., Pan, S., Najjar, R. G., Friedrichs, M. A. M., Bian, Z., Li, H. Y., & Hofmann,
1149 E. E.: Riverine Carbon Cycling Over the Past Century in the Mid-Atlantic Region of the
1150 United States, *J. Geophys. Res. Biogeosciences*, 126, 5, 1–21,
1151 <https://doi.org/10.1029/2020JG005968>, 2021.
- 1152 Yau, Y. Y., Baker, D. M., & Thibodeau, B.: Quantifying the Impact of Anthropogenic
1153 Atmospheric Nitrogen Deposition on the Generation of Hypoxia under Future Emission
1154 Scenarios in Chinese Coastal Waters, *Environ. Sci. Technol.*, 54, 7, 3920–3928,
1155 <https://doi.org/10.1021/acs.est.0c00706>, 2020.
- 1156 Yip, S., Ferro, C. A. T., Stephenson, D. B., & Hawkins, E.: A Simple, coherent framework for
1157 partitioning uncertainty in climate predictions, *J. Clim.*, 24, 17, 4634–4643,
1158 <https://doi.org/10.1175/2011JCLI4085.1>, 2011.
- 1159 Zahran, A. R., Zhang, Q., Tango, P., & Smith, E. P.: A water quality barometer for Chesapeake
1160 Bay: Assessing spatial and temporal patterns using long-term monitoring data, *Ecol. Indic.*,
1161 140, April, 109022, <https://doi.org/10.1016/j.ecolind.2022.109022>, 2022.
- 1162 Zhang, Q., Murphy, R. R., Tian, R., Forsyth, M. K., Trentacoste, E. M., Keisman, J., & Tango, P.
1163 J.: Chesapeake Bay’s water quality condition has been recovering: Insights from a
1164 multimetric indicator assessment of thirty years of tidal monitoring data, *Sci. Total Environ.*,
1165 637–638, 1617–1625, <https://doi.org/10.1016/j.scitotenv.2018.05.025>, 2018.
- 1166 Zhang, W., Dunne, J. P., Wu, H., & Zhou, F.: Regional projection of climate warming effects on
1167 coastal seas in east China, *Environ. Res. Lett.*, 17, 7, 074006, <https://doi.org/10.1088/1748-9326/ac7344>, 2022.

<https://doi.org/10.5194/egusphere-2022-1028>

Preprint. Discussion started: 20 October 2022

© Author(s) 2022. CC BY 4.0 License.



1169 Zhang, W., Moriarty, J. M., Wu, H., & Feng, Y.: Response of bottom hypoxia off the Changjiang
1170 River Estuary to multiple factors: A numerical study, *Ocean Model.*, 159, May 2020,
1171 <https://doi.org/10.1016/j.ocemod.2021.101751>, 2021.
1172



1173 **Tables and Figures**

1174

1175 **Table 1.** Experiments conducted to quantify future changes in Annual Hypoxic Volume (AHV).

1176

Experiment Name	Number of ESMS	Number of downscaling techniques	Number of watershed models	Number of simulations
Multi-Factor	5 ^a	2 (MACA and BCSD)	2 (DLEM and Phase 6)	20 ^b
Management	5 ^a	1 (MACA)	1 (Phase 6)	5 ^c
All-ESMs	20	1 (MACA)	1 (DLEM)	20

1177 ^aCorresponding to the KKZ-selected subset of five ESMS: Center, Cool/Dry, Hot/Wet, Cool/Wet, and Hot/Dry for both MACA
1178 and BCSD downscaled model outputs.

1179 ^bAdditional scenarios were simulated for the Multi-Factor experiment as needed (for the Center and Hot/Wet ESMS) to
1180 accurately partition uncertainty in model outcomes.

1181 ^cAn additional scenario simulated the effects of future management conditions without climate change impacts.



1182 **Table 2:** Nash-Sutcliffe efficiencies of the DLEM and Phase 6 Watershed Models at the most
1183 downstream stations of three major rivers, for monthly estimates of discharge and nutrient
1184 loading over the period 1991-2000. Nash-Sutcliffe efficiencies equal to one are indicative of
1185 perfect model skill and negative values indicate that error variance exceeds the observed
1186 variance.

Major River	Freshwater Discharge		Nitrate Loading		Organic Nitrogen Loading	
	DLEM	Phase 6	DLEM	Phase 6	DLEM	Phase 6
Susquehanna	0.74	0.88	0.60	0.78	0.37	0.12
Potomac	0.59	0.90	0.32	0.87	0.34	-0.69
James	0.59	0.92	-1.05	0.42	0.51	0.72

1187



1188 **Table 3:** Model skill metrics over the reference period (1991-2000)

Variable	Depth	Watershed model	ChesROMS-ECB estimate	Observed estimate ^a	Bias	RMSD
O ₂ [mg L ⁻¹]	Surface	DLEM	7.9 ± 2.3	9.3 ± 2.0	-1.4	2.2
		Phase 6	8.0 ± 2.3		-1.4	2.2
	Bottom	DLEM	6.1 ± 3.5	5.7 ± 3.5	0.4	1.7
		Phase 6	6.2 ± 3.4		0.5	1.6
NO ₃ [mmol N m ³]	Surface	DLEM	0.32 ± 0.36	0.23 ± 0.33	0.09	0.23
		Phase 6	0.30 ± 0.37		0.06	0.22
	Bottom	DLEM	0.27 ± 0.33	0.14 ± 0.24	0.13	0.25
		Phase 6	0.25 ± 0.33		0.11	0.23
DON [mmol N m ³]	Surface	DLEM	0.27 ± 0.05	0.28 ± 0.08	-0.00	0.08
		Phase 6	0.32 ± 0.08		0.05	0.12
	Bottom	DLEM	0.27 ± 0.05	0.26 ± 0.08	0.00	0.08
		Phase 6	0.31 ± 0.08		0.04	0.11
Primary Production [mg C m ⁻² d ⁻¹]	Water	DLEM	1146 ± 154 ^b	957 ± 287	189	N/A
	Column	Phase 6	1133 ± 129		176	
AHV [km ³ d]	Water	DLEM	987 ± 254	785 ± 201	202	250
	Column	Phase 6	906 ± 199		121	212

1189 ^aObserved estimates and standard deviations for O₂, NO₃, and DON are from the WQMP at 20 main stem stations. Observed
 1190 estimate and standard error for primary production are derived from Harding et al. (2002), averaged over Feb-Nov for the years
 1191 1982-1998. Observed estimate and standard deviation for AHV is derived by applying a weighted-distance interpolation model to
 1192 observed O₂ at a limited number of stations (Bever et al., 2013).

1193 ^bModeled primary production is computed only over Feb-Nov for comparison with the observed estimate.



1194 **Table 4:** Annual average and standard deviations of reference (1991-2000) and climate scenario
 1195 (2046-2055) watershed loadings and estuarine hypoxia.

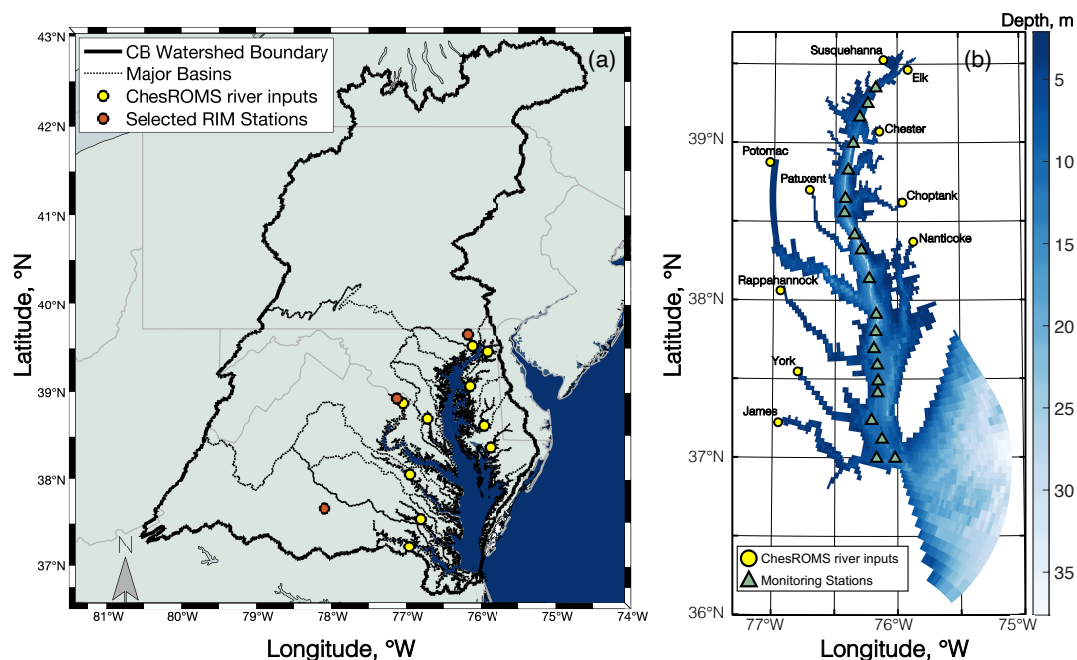
Watershed Freshwater Discharge [km ³ y ⁻¹]					
Watershed Model	DLEM		Phase 6		Phase 6 with Management
1990s	84 ± 26		72 ± 21		74 ± 21
2050s Downscaling	MACA	BCSD	MACA	BCSD	MACA
Center	87 ± 28	74 ± 24	78 ± 21	80 ± 22	79 ± 21
Cool/Dry	76 ± 24	75 ± 24	67 ± 19	77 ± 22	68 ± 19
Hot/Wet	84 ± 29	86 ± 29	79 ± 22	77 ± 21	80 ± 22
Hot/Dry	77 ± 25	74 ± 23	70 ± 20	68 ± 20	72 ± 20
Cool/Wet	93 ± 29	95 ± 30	83 ± 22	80 ± 22	84 ± 22
ESM Average	84 ± 27	81 ± 26	75 ± 21	76 ± 21	77 ± 21
Watershed Nitrogen Loading [10 ⁹ gN y ⁻¹]					
Watershed Model	DLEM		Phase 6		Phase 6 with Management
1990s	151 ± 49		147 ± 46		87 ± 28
2050s Downscaling	MACA	BCSD	MACA	BCSD	MACA
Center	159 ± 46	138 ± 41	177 ± 63	192 ± 75	103 ± 36
Cool/Dry	137 ± 39	132 ± 38	133 ± 36	166 ± 53	78 ± 23
Hot/Wet	157 ± 48	153 ± 45	183 ± 66	184 ± 68	105 ± 37
Hot/Dry	149 ± 45	138 ± 41	146 ± 42	140 ± 40	86 ± 26
Cool/Wet	159 ± 43	181 ± 62	301 ± 186	352 ± 244	156 ± 85
ESM Average	152 ± 43	148 ± 48	188 ± 110	207 ± 139	105 ± 53
Annual Hypoxic Volume [km ³ d]					
Watershed Model	DLEM		Phase 6		Phase 6 with Management
1990s	987 ± 254		904 ± 171		449 ± 144
2050s Downscaling	MACA	BCSD	MACA	BCSD	MACA
Center	1072 ± 233	985 ± 250	926 ± 152	938 ± 152	470 ± 131
Cool/Dry	994 ± 252	975 ± 257	885 ± 177	961 ± 170	429 ± 148
Hot/Wet	1094 ± 247	1059 ± 249	931 ± 156	928 ± 171	480 ± 131
Hot/Dry	1075 ± 263	996 ± 259	893 ± 164	871 ± 165	442 ± 141
Cool/Wet	1011 ± 204	1081 ± 238	969 ± 170	997 ± 203	507 ± 138
ESM Average	1049 ± 234	1019 ± 244	921 ± 160	939 ± 171	466 ± 135

1196

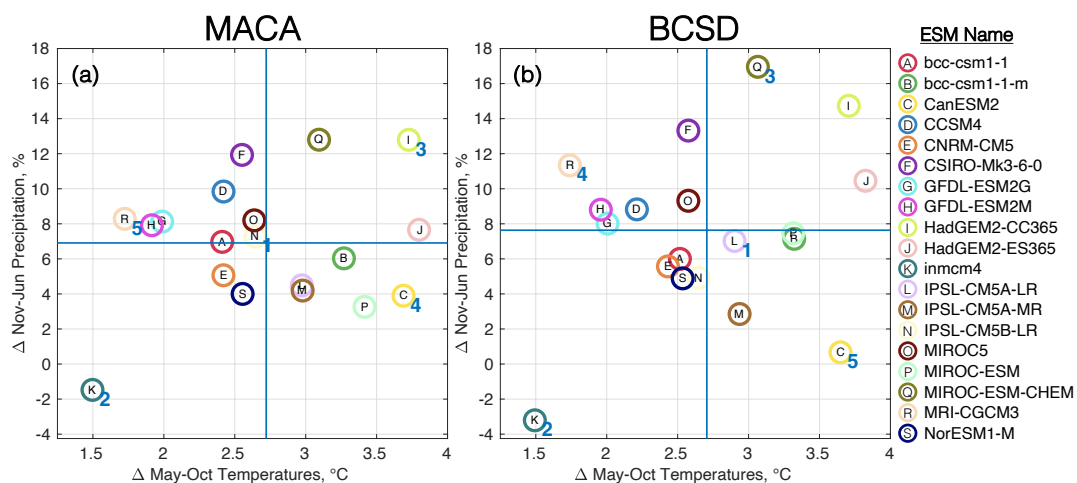


1197 **Table 5:** Average \pm standard error in Δ AHV (%) holding scenario effects (ESM, Downscaling
1198 Method, Watershed Model) constant.

Scenario Factor	Effect	Δ AHV, %
ESM	Center	4.4 ± 5.4
	Cool/Dry	0.9 ± 4.3
	Hot/Wet	6.7 ± 6.2
	Hot/Dry	1.4 ± 3.6
	Cool/Wet	8.3 ± 6.5
Downscaling	MACA	4.8 ± 6.0
	BCSD	3.9 ± 5.9
Watershed Model	DLEM	5.6 ± 7.5
	Phase 6	3.1 ± 3.8



1199
1200 **Figure 1:** (a) Map showing the extent of the Chesapeake Bay watershed boundary, major basins,
1201 River Input Monitoring (RIM) stations for the Susquehanna, Potomac, and James Rivers (red
1202 red circles), and ChesROMS river input locations (yellow circles). (b) Bathymetry of the
1203 ChesROMS-ECB model domain, river input locations (yellow circles), and 20 CBP main stem
1204 monitoring stations (green triangles).



1205

1206

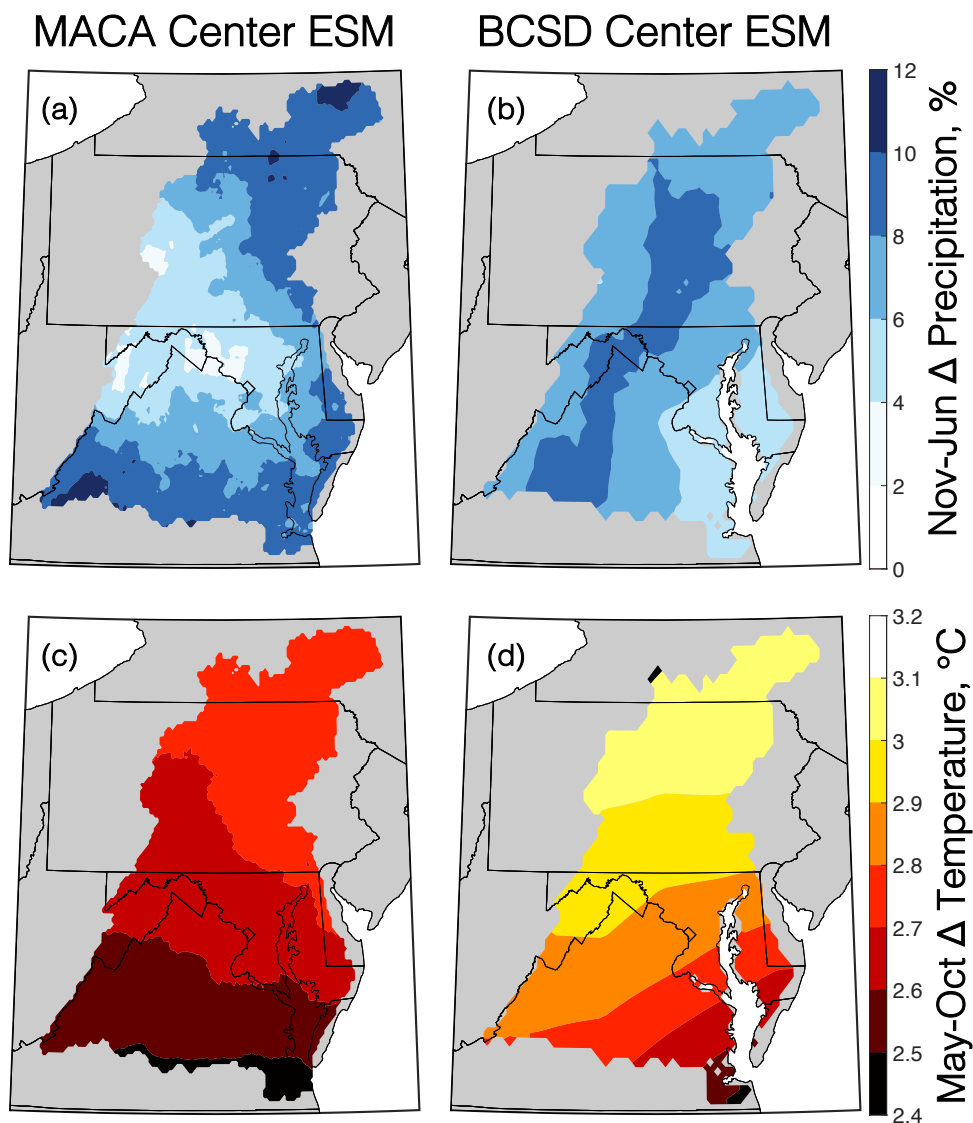
1207 **Figure 2:** Relative changes in May-October temperatures and November-June precipitation over

1208 the Chesapeake Bay watershed for an ensemble of ESMs (circled letters) downscaled using (a)

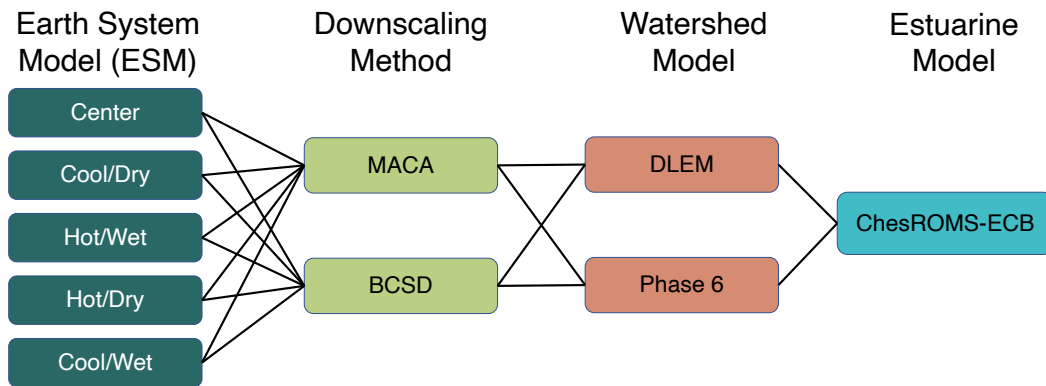
1209 MACA and (b) BCSD methodologies. Horizontal and vertical blue lines correspond to the

1210 ensemble average changes in temperature and precipitation. Numbers adjacent to particular

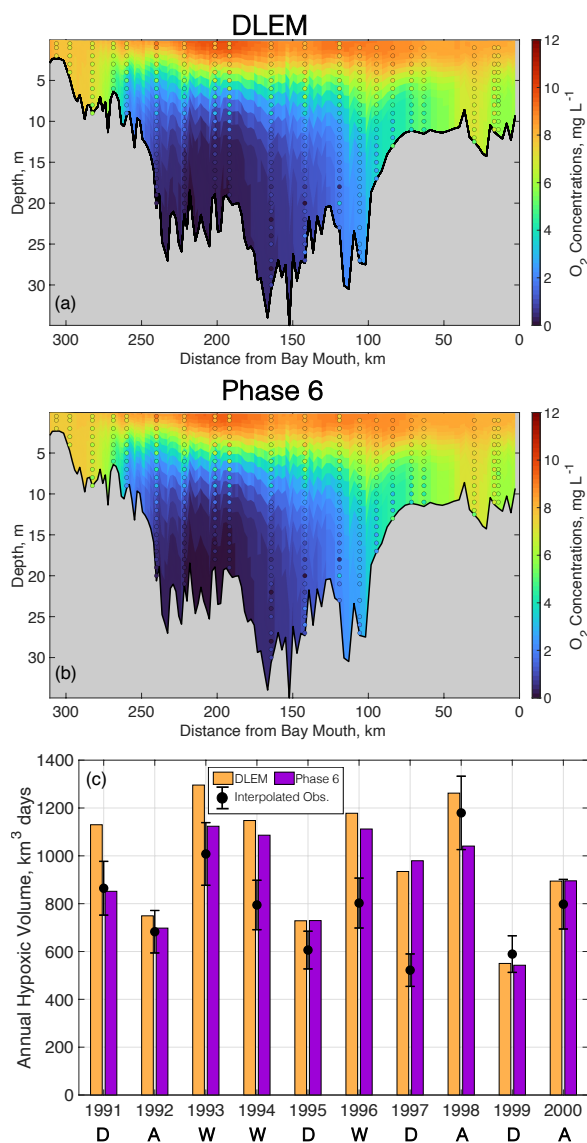
ESMs in both panels denote the order in which the first five were selected by the KKZ algorithm.



1211
1212 **Figure 3:** Changes in November to June precipitation (a, b) and May to October temperatures (c,
1213 d) for the MACA (a, c) and BCSD (b, d) Center ESMs between mid-century (2046-2055) and the
1214 reference period (1991-2000).



1215
1216 **Figure 4:** Diagram of Multi-Factor experimental design, comprising a total of 20 model
1217 scenarios.



1218

1219

Figure 5: ChesROMS-ECB skill for average summer (Jun-Aug) O₂ profiles at main stem

monitoring locations using watershed inputs from (a) DLEM and (b) Phase 6 over the reference

period 1991-2000. (c) Modeled AHV using DLEM and Phase 6 compared to interpolated

observations (error bars denote RMS percent error) over the reference period 1991-2000.

Average hydrologic conditions are noted below corresponding years and signify dry (D), average

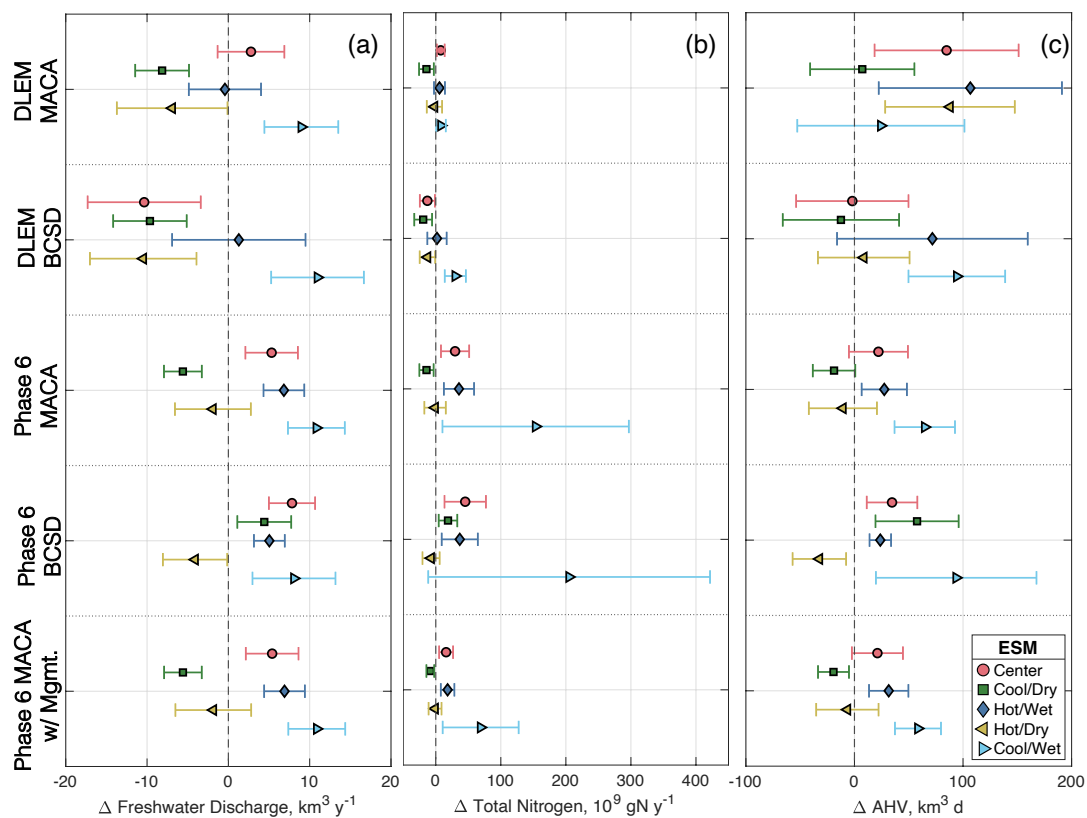
1223

(A), or wet (W) years.

1224



1225



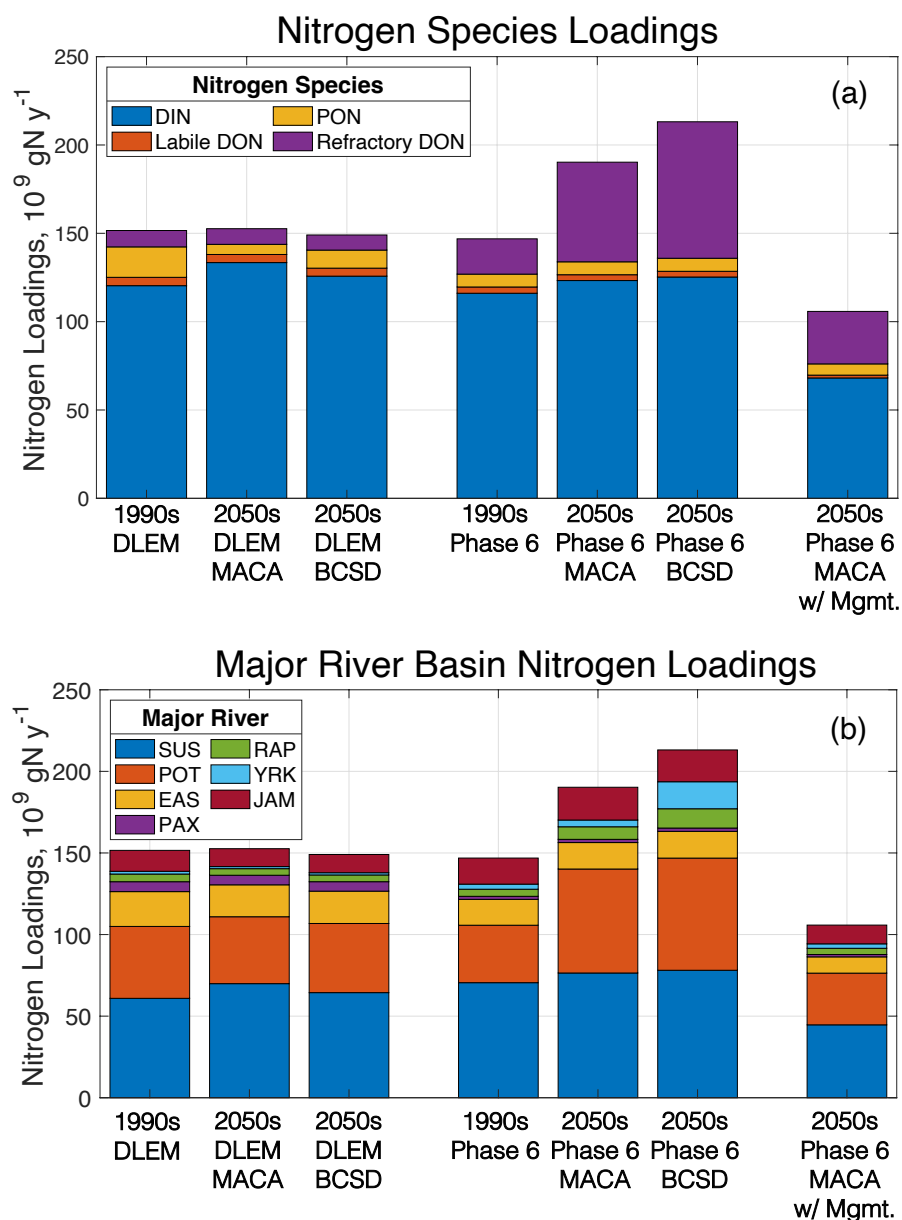
1226

1227

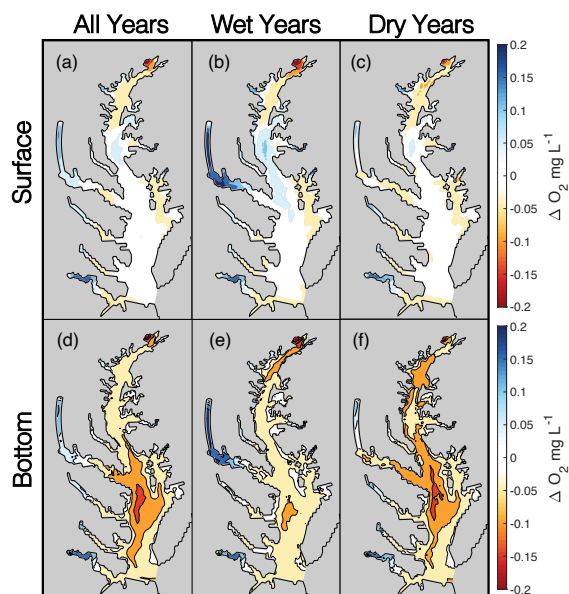
1228

1229

Figure 6: Mean and standard deviations of changes to freshwater discharge (a), total nitrogen loadings (b), and annual hypoxic volume (c) for Multi-Factor and Management experiments.



1230
 1231 **Figure 7:** Average TN loadings among ESM scenarios for reference scenarios and various
 1232 components of the Multi-Factor and Management experiments. TN loadings divided by (a)
 1233 nitrogen species component: dissolved inorganic nitrogen (DIN), particulate organic nitrogen
 1234 (PON), dissolved organic nitrogen (DON), and refractory dissolved organic nitrogen, and (b) by
 1235 major river basin (SUS = Susquehanna, RAP = Rappahannock, POT = Potomac, YRK = York,
 1236 EAS denoting eastern shore rivers including the Elk, Chester, Choptank, and Nanticoke, JAM =
 1237 James, PAX = Patuxent).



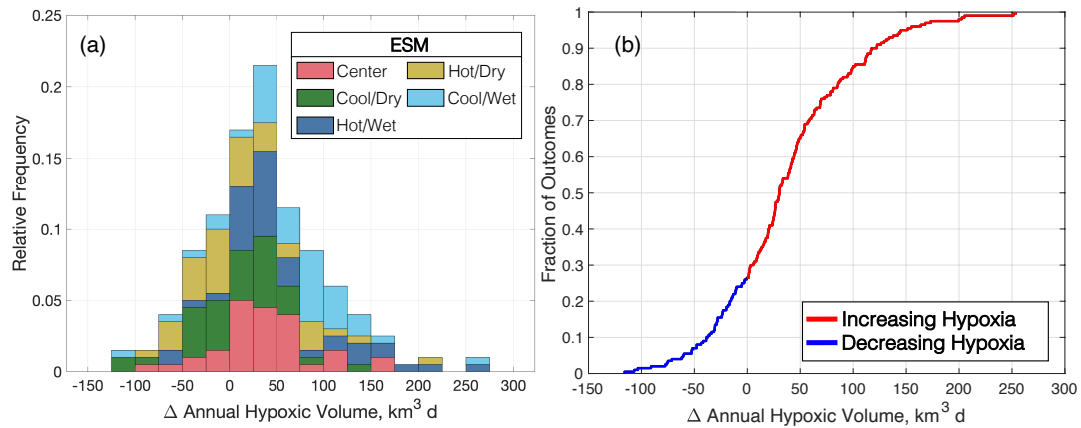
1238

1239

1240

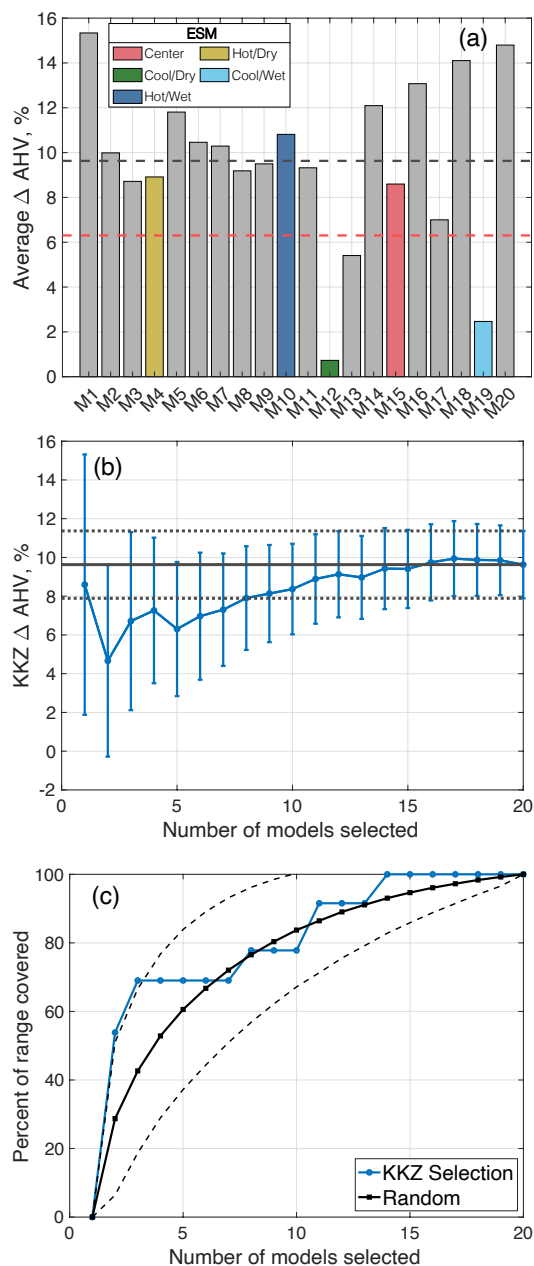
1241

Figure 8: Average O₂ changes in Multi-Factor experiment scenarios at the surface (a-c) and bottom (d-f). Columns correspond to average changes for all years (a, d) as well as hydrologically wet (b, e) and dry (c, f) years.

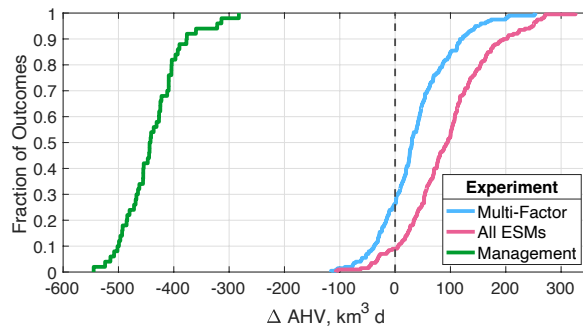


1242
1243
1244

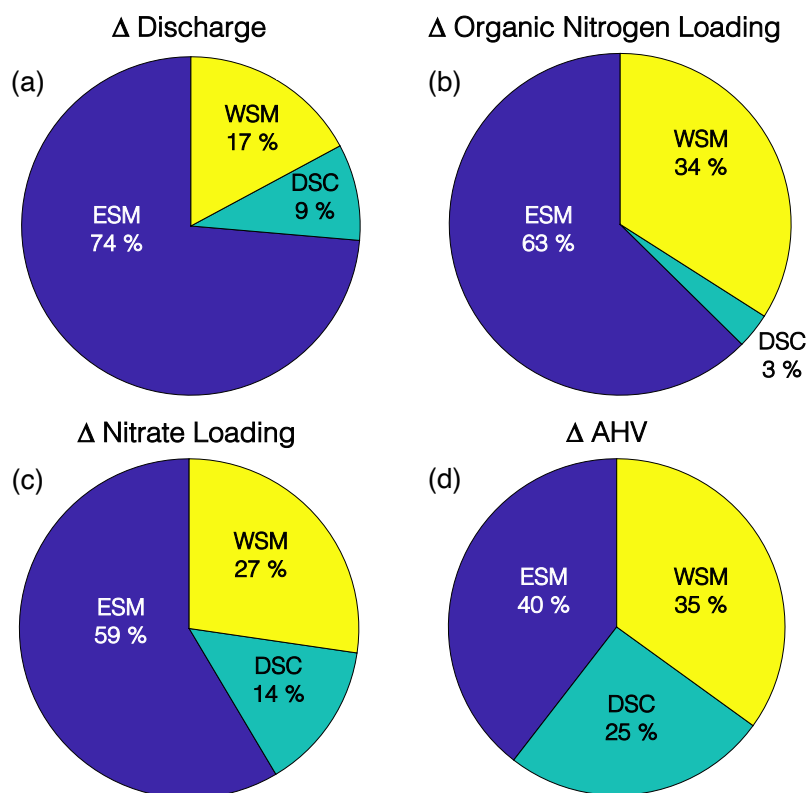
Figure 9: Summary of Multi-Factor experiment results for changes to annual hypoxic volume, expressed as a histogram of relative frequencies (a) and an empirical cumulative distribution (b).



1245
 1246 **Figure 10:** (a) Δ AHV for the All-ESMs experiment. Red dashed line denotes the multi-model
 1247 average of five KKZ-selected ESMs; black dashed line denotes the full 20-model average. (b)
 1248 Δ AHV and standard errors as estimated by increasing number of KKZ-selected ESMs. Black
 1249 lines correspond to 20-model average (solid) and associated standard errors (dotted) from the
 1250 All-ESMs experiment. (c) Percent of Δ AHV range covered by sequentially increasing the
 1251 number of KKZ-selected ESMs. Black lines correspond to the range (solid) and associated
 1252 standard error (dashed) of estimates chosen by randomly selecting ESMs.



1253
1254 **Figure 11:** Summary of all experiment results for change in Annual Hypoxic Volume (Δ AHV),
1255 expressed as a cumulative distribution function. Black dashed vertical line corresponds to no
1256 change in AHV.



1257
1258 **Figure 12:** Percent contribution to uncertainty from Earth System Model (ESM), downscaling
1259 methodology (DSC), and watershed model (WSM), for estimates of (a) discharge, (b) organic
1260 nitrate loading, (c) nitrate loading, and (d) change in annual hypoxic volume (Δ AHV).